 CMES, vol.81, no.2, pp.119-156, 2011

Coupled Wavenumbers in an Infinite Flexible Fluid-Filled Circular Cylindrical Shell : Comparison between Different Shell Theories

M. V. Kunte[1], **and Venkata R. Sonti**[1]

Abstract: Analytical expressions are found for the wavenumbers in an infinite flexible *in vacuo* / fluid-filled circular cylindrical shell based on different shell-theories using asymptotic methods. Donnell-Mushtari theory (the simplest shell theory) and four higher order theories, namely Love-Timoshenko, Goldenveizer-Novozhilov, Flügge and Kennard-simplified are considered. Initially, *in vacuo* and fluid-coupled wavenumber expressions are presented using the Donnell-Mushtari theory. Subsequently, the wavenumbers using the higher order theories are presented as perturbations on the Donnell-Mushtari wavenumbers. Similarly, expressions for the resonance frequencies in a finite shell are also presented, using each shell theory. The basic differences between the theories being what they are, the analytical expressions obtained from the five theories allow one to see how these differences propagate into the asymptotic expansions. Also, they help to quantify the difference between the theories for a wide range of parameter values such as the frequency range, circumferential order, thickness ratio of the shell, etc.

Keywords: shell, shell theories, wave propagation, fluid filled, fluid loading, cylindrical shell, wavenumbers, asymptotics, perturbation methods

1 Introduction

Curved shells are widely used structural elements which find applications in diverse systems such as pipelines, aircraft and vehicle panels, fan-blades, etc. Because of the complexity involved in deriving the equations of motion in such structures, various simplifications are made at different steps in the derivation of these equations, resulting in the different shell theories. The degree of accuracy depends on the severity of the simplifications made in the derivation. And depending on the nature

[1] Vibro-Acoustics Lab, Facility for Research in Technical Acoustics, Department of Mechanical Engineering, Indian Institute of Science, Bangalore - 560012, India

of the loading and the frequency regime considered, a simpler theory may also be sufficient.

In particular, in the area of structural acoustics, while computing sound radiation using fully coupled theories, wavenumbers as functions of frequency are often required. In the literature, these wavenumbers are computed using iterative numerical techniques as has been done by Venkatesham, Pathak, and Munjal (2007). If the wavenumber is given in a closed form expression, then it becomes very convenient. One may also wish to know the degree of accuracy of the shell theory that one is using and further how the inaccuracy propagates when one does asymptotic expansions using that theory. A valuable treatise along these lines is that by Leissa (1973), where natural frequency parameters were given for various shell configurations using various shell theories having varying degrees of accuracies. In this document we extend that idea by comparing wavenumbers in *in vacuo* and fluid-filled shells over a wide frequency range using five commonly accepted shell theories. Here, the focus is how these five theories compare with each other and how the asymptotic expansions of the wavenumbers also reflect the comparison.

The five shell theories are, namely the Donnell-Mushtari, the Love-Timoshenko, the Goldenveizer-Novozhilov, the Flügge and the simplified Kennard theory. While there are a number of shell theories available in the literature, not all of them are entirely unrelated; a lot of theories invoke similar or identical assumptions and simplifications in their development as noted by Leissa (1973). Donnell-Mushtari (DM) theory was originally presented by Donnell (1933) and Mushtari (1938) (in Russian). The Love-Timoshenko theory was presented by Love (1944) and Timoshenko (1959). The Goldenveizer-Novozhilov theory was presented originally by Goldenveizer (1961) and Novozhilov (1964). The Flügge shell theory was presented in the book by Flügge (1962). Finally, the shell theory originally presented by Epstein (1942) was rederived and simplified by Kennard (1953, 1955, 1956, 1958). These theories were compiled by Leissa (1973) and presented as modifications on the equations of motion for the DM theory.

In recent times, the DM theory has been used to model the dynamics of a fluid-filled shell by Sarkar and Sonti (2007b, 2009). The coupled wavenumbers for the axisymmetric and the beam modes, respectively, were presented. Generalized expansions for the *in vacuo* wavenumbers in a circular cylindrical shell were later obtained by Kunte, Sarkar, and Sonti (2011) using DM theory, treating the circumferential order as a parameter. All the results in the above papers [Sarkar and Sonti (2007b, 2009); Kunte, Sarkar, and Sonti (2011)] were obtained using a perturbation approach; a frequency-scaling parameter and/ or a fluid-loading parameter were defined and used as asymptotic expansion parameters to obtain the closed-form expressions for the wavenumbers.

In this paper, we extend this approach by obtaining the dispersion relation for each of the shell theories and provide closed form expressions for wavenumbers using the asymptotic methods. The expressions themselves are presented as perturbations to those obtained from DM theory. These solutions are then compared with each other in different frequency regimes to be able to quantify the difference between the theories.

Next, a finite shell is considered and resonance frequencies corresponding to the Shear-diaphragm (SD) boundary conditions at both ends are found for the five theories. Leissa (1973) has presented numerical results for the resonance frequencies for a few thickness ratios and length ratios. Here, we obtain asymptotic expansions for the resonance frequencies for the *in vacuo* shells using each of the theories.

The paper is organized as follows. In Section 2, we highlight the differences between the shell theories. We present the equations of motion for the DM theory in a matrix form along with the correction terms for the higher-order theories. In Section 3, we consider the *in vacuo* infinite shell. We present the asymptotic expansions found earlier [Kunte, Sarkar, and Sonti (2011)] for the wavenumbers in an *in vacuo* shell based on the DM theory. The correction term to the DM wavenumber for each of the other four theories is then presented and the results are compared. In Section 4, the fluid-loading term is added to the equations of motion. Again, the results for the DM theory are presented, followed by the results for each of the four theories. In Section 5, an *in vacuo* finite shell with SD-SD boundary conditions at each end is considered, with and without fluid-loading. Asymptotic expansions for the resonance frequencies in the axisymmetric mode are found for each theory and presented in the same fashion as the earlier sections. It is difficult to make a prediction regarding the accuracy of an asymptotic expansion *a priori*. Hence, throughout this manuscript, a trial and error approach is used to obtain asymptotic expansions that are both elegant and accurate.

At this point, we make a few observations regarding the terminology employed in this paper. Since the wavenumber expansions from the different theories are presented as perturbations on the corresponding DM theory expansions, the four other theories, namely the Love-Timoshenko, the Goldenveizer-Novozhilov, the Flügge and the simplified Kennard theory will henceforth be referred to as the higher order theories or HOTs. Also, the acronyms LT, GN, F and K stand for the Love-Timoshenko, the Goldenveizer-Novozhilov, the Flügge and the Kennard-simplified theories, respectively.

2 Theory

2.1 Differences in the shell theories

The different steps in the derivation of the equations of motion of a curved shell are available in Leissa (1973) but we list them here for clarity. These are as follows:

1. Derivation of the strain-displacement relations.
2. Writing the stress-strain relations using Hooke's law.
3. Integrating the stresses to obtain the force and moment resultants.
4. Using these resultants in the equilibrium equations to obtain the equations of motion in terms of the displacements.

In general, according to the first assumption in the Love-Kirchoff hypothesis in the theory of small displacements of thin shells, the thickness of the shell is considered small in comparison to the other dimensions. Thus, at various points in the derivation, this assumption may be invoked differently, which results in the different theories. In the strain-displacement relations obtained by the Love-Timoshenko theory, terms of the form $\left(1+\frac{z}{R}\right)\approx 1$, where z is the radial coordinate and R is the radius of curvature. In the Goldenveizer-Novozhilov and Flügge theories, this term is retained as it is. The DM theory is one of the simplest of the shell theories and carries over the assumption from the Love-Timoshenko theory. An additional simplification in DM theory is that the tangential displacements and their derivatives are neglected in the equations for the changes in curvature and twist at the midsurface (bending component of the strains) [Leissa (1973)].

The next set of simplifications are made in the integration of the stresses to obtain the force and moment resultants. Since the z/R term is already removed in the Love-Timoshenko and the DM theories, no further simplification is made. In the Flügge theory, the term $(1+z/R)$ is expanded in a Taylor series about $z=0$ and truncated at the third order, and then integrated. In the Goldenveizer-Novozhilov theory, a strain-energy integral is defined, and the Kirchoff hypothesis is not applied [Leissa (1973)]. This results in force and moment resultants that are identical to those obtained by the Love-Timoshenko theories except for the force resultants $N_{\alpha\beta}$ and $N_{\beta\alpha}$. This does away with the inconsistencies in the DM and Love-Timoshenko theories that $N_{\alpha\beta}=N_{\beta\alpha}$ though a similar inconsistency ($M_{\alpha\beta}=M_{\beta\alpha}$) is not removed. The Flügge theory manages to elminate both inconsistencies, i.e., $N_{\alpha\beta}\neq N_{\beta\alpha}$ and $M_{\alpha\beta}\neq M_{\beta\alpha}$.

These results are then substituted in the differential equations of equilibrium to obtain the final equations of motion. A final simplification in the DM theory is

that terms containing the shear resultants in the normal and tangential directions are neglected in the equilibrium equations in the two tangential directions while the other equations remain the same.

The Kennard-simplified theory of shells originated differently. This theory was obtained by specializing equations of motion derived directly from three-dimensional elasticity theory to the case of circular cylindrical shells. The original equations derived by Epstein were obtained by expanding stresses and displacements with respect to the radial coordinate z.

2.2 Equations of motion

Consider an infinite circular cylindrical shell of thickness h, radius a and made of a material with density ρ_s, Young's modulus E and Poisson's ratio ν. The partial differential equations of motion for such a shell have been presented by Fuller (1983) in the matrix form (that includes the fluid loading term). The equations are presented in the form

$$\mathbf{L}\{\mathbf{u}\} = \left(\mathbf{L}_{\mathrm{DM}} + k_\beta \mathbf{L}_{\mathrm{mod}}\right)\{\mathbf{u}\} = 0, \tag{1}$$

where $\mathbf{L}_{\mathrm{DM}}$ is the differential operator corresponding to the DM theory, $\mathbf{L}_{\mathrm{mod}}$ contains the modifications corresponding to the HOTs and k_β is given by $k_\beta = \beta^2 = h^2/(12a^2)$. $\{\mathbf{u}\}$ is the vector of displacements. The displacement profiles are substituted in the above equation following Fuller and Fahy (1982) as

$$\begin{aligned} u &= U\cos(n\theta)\mathrm{e}^{\mathrm{i}(\kappa s-\omega t+\pi/2)},\\ v &= V\sin(n\theta)\mathrm{e}^{\mathrm{i}(\kappa s-\omega t)},\\ w &= W\cos(n\theta)\mathrm{e}^{\mathrm{i}(\kappa s-\omega t)}, \end{aligned}$$

where κ is the wavenumber in the axial direction and ω is the frequency of excitation. Thus, Eq. (1) is now non-dimensionalized by defining the non-dimensional variables $\Omega = \omega a/c_L, \beta = h/(a\sqrt{12})$ and simplified to give

$$[\mathbf{D}]\{\mathbf{U}\} = \left[\mathbf{D}_{\mathrm{DM}} + k_\beta \mathbf{D}_{\mathrm{mod}}\right]\{\mathbf{U}\} = 0, \tag{2}$$

where c_L is the quasi-longitudinal wave speed given by $c_L = \sqrt{\frac{E}{\rho_s(1-\nu^2)}}$, $\{\mathbf{U}\}$ is the vector of displacement amplitudes and the matrix $[\mathbf{D}_{\mathrm{DM}}]$ is given by

$$\begin{bmatrix} \mathbf{D}_{11} & \frac{1}{2}\mathrm{i}\kappa n(1+\nu) & \mathrm{i}\nu\kappa \\ \frac{1}{2}\kappa n(1+\nu) & \mathbf{D}_{22} & -n \\ -\nu\kappa & n & \mathbf{D}_{33} \end{bmatrix},$$

where

$$\mathbf{D}_{11} = \frac{1}{2}\mathrm{i}\left(\nu n^2 - 2\kappa^2 - n^2 + 2\Omega^2\right),$$
$$\mathbf{D}_{22} = \frac{1}{2}\nu\kappa^2 - \frac{1}{2}\kappa^2 + \Omega^2 - n^2,$$
$$\mathbf{D}_{33} = 1 + \beta^2\kappa^4 + 2\beta^2\kappa^2 n^2 + \beta^2 n^4 - \Omega^2 + \mathscr{F},$$

and $\mathscr{F}$ is the fluid-loading term which will be defined later.
The matrix $\mathbf{D}_{\mathrm{mod}}$ is given below for each theory,

$$\mathbf{D}_{\mathrm{mod}}^{\mathrm{LT}} = \begin{bmatrix} 0 & 0 & 0 \\ 0 & \nu\kappa^2 - \kappa^2 - n^2 & -n\left(\kappa^2 + n^2\right) \\ 0 & n\left(2\kappa^2 - \nu\kappa^2 + n^2\right) & 0 \end{bmatrix},$$

$$\mathbf{D}_{\mathrm{mod}}^{\mathrm{GN}} = \begin{bmatrix} 0 & 0 & 0 \\ 0 & 2\nu\kappa^2 - 2\kappa^2 - n^2 & -n\left(2\kappa^2 - \nu\kappa^2 + n^2\right) \\ 0 & n\left(2\kappa^2 - \nu\kappa^2 + n^2\right) & 0 \end{bmatrix},$$

$$\mathbf{D}_{\mathrm{mod}}^{\mathrm{F}} = \begin{bmatrix} \frac{1}{2}\mathrm{i}n^2(\nu - 1) & 0 & \frac{1}{2}\mathrm{i}\kappa\left(2\kappa^2 - n^2 + \nu n^2\right) \\ 0 & \frac{3}{2}\kappa^2(\nu - 1) & \frac{1}{2}n\kappa^2(-3 + \nu) \\ -\frac{1}{2}\kappa\left(2\kappa^2 - n^2 + \nu n^2\right) & -\frac{1}{2}n\kappa^2(-3 + \nu) & 1 - 2n^2 \end{bmatrix},$$

$$\mathbf{D}_{\mathrm{mod}}^{\mathrm{K}} = \begin{bmatrix} 0 & 0 & 0 \\ 0 & 0 & -\frac{3}{2}\frac{n\nu\left(-1+n^2\right)}{-1+\nu} \\ 0 & 0 & \frac{(2+\nu)}{2(1-\nu)} - \frac{1}{2}\frac{n^2(\nu-4)}{-1+\nu} \end{bmatrix}.$$

From Eq. (2), for the vector of displacement amplitudes $\{\mathbf{U}\}$ to have a non-trivial solution, the determinant of matrix $[\mathbf{D}]$ must be equal to zero. This gives the dispersion relation.

3 *In vacuo* infinite shell

The dispersion relation for an *in vacuo* shell is obtained by setting the fluid-loading term $\mathscr{F}$ to zero in Eq. (2) and then equating the determinant of the matrix $[\mathbf{D}]$ to zero. The expressions for the *in vacuo* wavenumbers are found using a regular perturbation approach.

Initially, the wavenumbers in the axisymmetric mode ($n = 0$) are found. Subsequently, for a general value of n, in order to obtain an elegant expression for the wavenumber from which it is easy to derive a physical understanding, the wavenumber and the frequency are suitably rescaled wherever necessary before finding the asymptotic expansions [Sarkar and Sonti (2009), Kunte, Sarkar, and Sonti (2010)].

3.1 Expansions for the axisymmetric mode ($n = 0$)

The simplification introduced in the *in vacuo* dispersion relation by setting $n = 0$ allows us to obtain expansions for all the wavenumbers without resorting to a frequency-rescaling approach. Thus, the expansions that are obtained are uniformly valid except at $\Omega = 1$ (for the flexural wavenumbers), which remains a singularity.

The wavenumbers are presented as perturbations to the corresponding wavenumbers for the DM theory; the correction terms for each of the HOTs, for each of the wavenumbers, are tabulated later. Thus, the wavenumbers in an isotropic shell in the $n = 0$ mode are as follows,

$$\begin{aligned}
\kappa_{\text{axial}} &= \Omega + \frac{1}{2}\frac{\nu^2\Omega}{\Omega^4\beta^2 - \Omega^2 + 1} + k_\beta C_{\text{axial}},\\
\kappa_{\text{torsional}} &= \sqrt{2}\Omega + \frac{1}{2}\nu\sqrt{2}\Omega + \frac{3}{8}\nu^2\sqrt{2}\Omega + k_\beta C_{\text{torsional}},\\
\kappa_{\text{prop}} &= \sqrt[4]{\left(\frac{\Omega^2-1}{\beta^2}\right)} + \frac{1}{4}\nu^2\frac{1}{\beta^2\sqrt[4]{\left(\frac{\Omega^2-1}{\beta^2}\right)}\left(\sqrt{\frac{\Omega^2-1}{\beta^2}} - \Omega^2\right)} + k_\beta C_{\text{prop}},\\
\kappa_{\text{nfb}} &= i\sqrt[4]{\left(\frac{\Omega^2-1}{\beta^2}\right)} + i\frac{1}{4}\nu^2\frac{1}{\beta^2\sqrt[4]{\left(\frac{\Omega^2-1}{\beta^2}\right)}\left(\sqrt{\frac{\Omega^2-1}{\beta^2}} - \Omega^2\right)} + k_\beta C_{\text{nfb}},
\end{aligned} \tag{3}$$

where setting $k_\beta = 0$ gives the wavenumber expansions for the DM theory.

The correction factors for each of the other theories are as shown in Table (1). The subscripts 'prop' and 'nfb' stand for the propagating bending wavenumber and the near-field bending wavenumber, respectively.

Fig. (1) shows a comparison of the asymptotic expressions given by the first two equations in Eq. (3) for the longitudinal and torsional wavenumbers in the axisymmetric mode with the numerical solutions (using the Flügge theory) for each of the four theories, while Fig. (2) shows a similar comparison for the propagating and near-field bending wavenumbers given by the last two of Eq. (3). In Fig. (1a) the asymptotic curve also exhibits the jump as in the numerical curve at $\Omega = 1$. It is not evident because of the low resolution of points used in the plot.

Correction term	Shell-theory			
	LT	GN	F	K
C_{axial}	0	0	0	0
$C_{\text{torsional}}$	$-\sqrt{2}\Omega$	$-2\sqrt{2}\Omega$	$-\frac{3}{2}\sqrt{2}\Omega$	0
C_{prop}	0	0	$-\frac{1}{4}\frac{1}{\left(\frac{\Omega^2-1}{\beta^2}\right)^{3/4}\beta^2}$	$-\frac{1}{4}\frac{1}{\left(\frac{\Omega^2-1}{\beta^2}\right)^{3/4}\beta^2}$
C_{nfb}	0	0	$-\mathrm{i}\frac{1}{4}\frac{1}{\left(\frac{\Omega^2-1}{\beta^2}\right)^{3/4}\beta^2}$	$-\mathrm{i}\frac{1}{4}\frac{1}{\left(\frac{\Omega^2-1}{\beta^2}\right)^{3/4}\beta^2}$

Table 1: Correction terms for the *in vacuo* wavenumbers for $n = 0$ for various shell theories.

All the dispersion curves have been plotted for $h/a = 0.05$, which is generally accepted to be the upper limit for the validity of thin shell theories [Leissa (1973)]. This corresponds to a value of $\beta = h/(a\sqrt{12}) = 0.0144$. The value of $k_\beta = \beta^2 = 2.07e-4$.

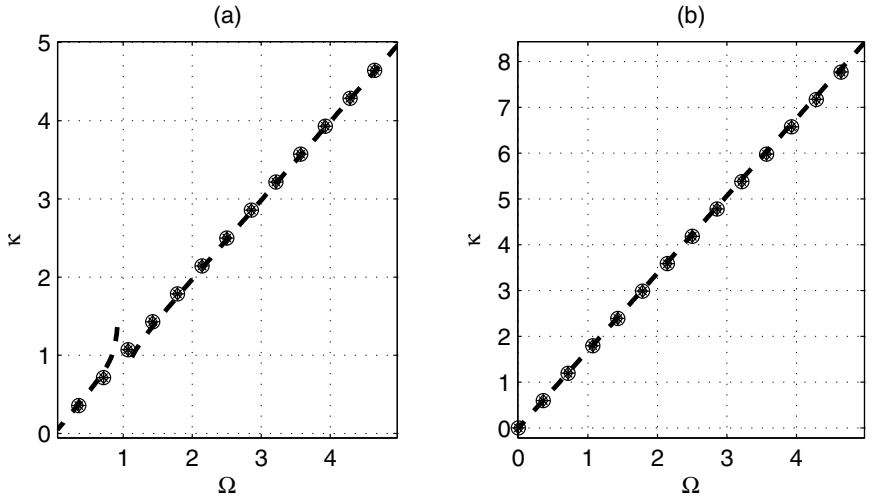

Figure 1: Comparison of the asymptotic solutions for the longitudinal and torsional wavenumbers for the axisymmetric mode ($n = 0$) for all the theories (Eq. (3a,b) - Donnell-Mushtari theory (Marker '+'), Love-Timoshenko theory (Marker 'o'), Goldenveizer-Novozhilov theory (Marker '×'), Flügge theory (Marker '∗') and Kennard simplified theory (Marker '⋄')) - with the corresponding numerical solution using the Flügge theory (Marker '- -') - $h/a = 0.05, \nu = 0.3, n = 0$, (a). Longitudinal wavenumber (b) Torsional wavenumber.

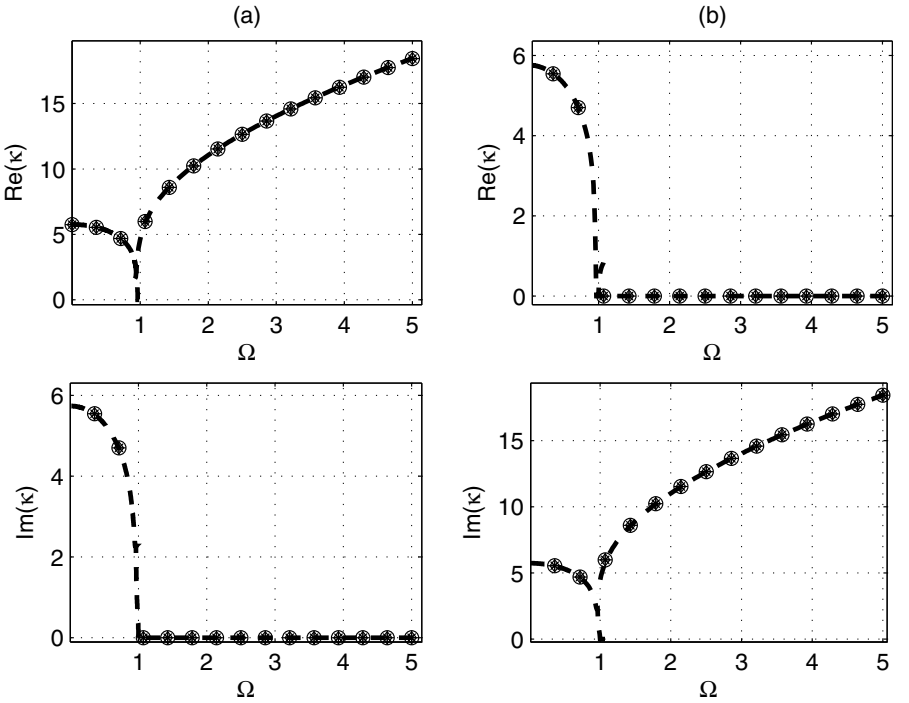

Figure 2: Comparison of the asymptotic solutions for the propagating and near-field bending wavenumbers for the axisymmetric mode ($n = 0$) for all the theories (Eq. (3c,d) - Donnell-Mushtari theory (Marker '+'), Love-Timoshenko theory (Marker 'o'), Goldenveizer-Novozhilov theory (Marker '$\times$'), Flügge theory (Marker '$*$') and Kennard simplified theory (Marker '$\diamond$')) - with the corresponding numerical solution using the Flügge theory (Marker '- -') - $h/a = 0.05, \nu = 0.3, n = 0$, (a). Propagating bending wavenumber (b). Near-field bending wavenumber.

3.2 High-frequency bending wavenumbers : $n \geq 1$

While obtaining wavenumber expansions that are valid for general circumferential orders, it is advantageous to use a frequency-scaling approach to find elegant expansions that are valid in separate frequency regimes. From prior experience with plates and shells, we know that the bending wavenumber $\kappa \propto \sqrt{\Omega}$. Thus, since we are interested in finding this wavenumber in the high-frequency region, we rescale the wavenumber and frequency as

$$\kappa = \frac{\kappa_{\text{rs}}}{\sqrt{\eta}}, \Omega = \frac{\Omega_{\text{rs}}}{\eta}, \tag{4}$$

where η is a fictitious scaling parameter which is of a magnitude much smaller than 1, $\kappa_{\rm rs}$ and $\Omega_{\rm rs}$ are the rescaled wavenumber and frequency, respectively, and are $\mathcal{O}(1)$ quantities. Next, a series expansion of the form $\kappa_{\rm rs} = \kappa_0 + \eta a_1 + \nu b_1 + k_\beta c_1$ is chosen for the rescaled wavenumber $\kappa_{\rm rs}$ and substituted in the dispersion equation. The dispersion relation is expanded in a Taylor series about $\nu = 0$, $\eta = 0$ and $k_\beta = 0$ and balanced at each order to solve for a_1, b_1 and c_1. This series can be truncated and higher powers eliminated since $k_\beta = \beta^2$ is a small quantity for thin shells and $\eta \ll 1$ by definition; thus, the series converges in an asymptotic sense.

The high frequency bending wavenumbers are as follows,

$$\kappa_{\rm prop} = \sqrt{\frac{\Omega}{\beta}} - \frac{1}{2}\frac{n^2}{\sqrt{\frac{\Omega}{\beta}}} + k_\beta C_1, \tag{5}$$

$$\kappa_{\rm nfb} = \mathrm{i}\sqrt{\frac{\Omega}{\beta}} + \frac{1}{2}\mathrm{i}\frac{n^2}{\sqrt{\frac{\Omega}{\beta}}} + k_\beta C_2, \tag{6}$$

where $\kappa_{\rm prop}$ and $\kappa_{\rm nfb}$ are the propagating bending and near-field bending wavenumbers, respectively. Setting $k_\beta = 0$ in the final solution for κ gives back the wavenumber for the Donnell-Mushtari theory. However, the coefficients C_1 and C_2 are found to be zero for all the theories, for both the propagating bending and the near-field bending wavenumbers. Thus, Eqs. (5, 6) are the same for all the theories. When the bilinear term $(k_\beta \eta)$ is included in the expansion for the wavenumber, the coefficient of this term also goes to zero implying that the correction from the more complicated theories is a higher-order effect.

Fig. (3) shows a comparison of the asymptotic expression for the propagating bending and near-field bending wavenumbers with the numerical solutions (using the Flügge theory) at high frequencies for each of the four theories.

3.3 Low-frequency bending wavenumbers : $n \geq 1$

For the low-frequency bending wavenumbers, the following variable transformation is used,

$$\kappa = \kappa_{rs}\sqrt{\eta},\ \Omega = \Omega_{rs}\eta,\ \beta = b\eta,\ k_\beta = \theta\eta^2. \tag{7}$$

A series expansion for $\kappa_{\rm rs}$ of the form $\kappa_{\rm rs} = \kappa_0 + \eta a_1 + \nu b_1 + \theta c_1$ is chosen. This expansion is substituted in the rescaled dispersion relation and balanced at each order to solve for the undetermined coefficients in the series expansion for $\kappa_{\rm rs}$. The resulting expansions in the unscaled variables for the propagating bending and near-field bending wavenumbers are shown below,

$$\kappa_{\rm prop} = \sqrt[4]{-n^2\left(-\Omega^2 - n^2\Omega^2 + n^6\beta^2\right)} - \frac{1}{4}\frac{-3\Omega^2 - 2n^2\Omega^2 + 4n^6\beta^2}{\sqrt[4]{-n^2\left(-\Omega^2 - n^2\Omega^2 + n^6\beta^2\right)}} + k_\beta C, \tag{8}$$

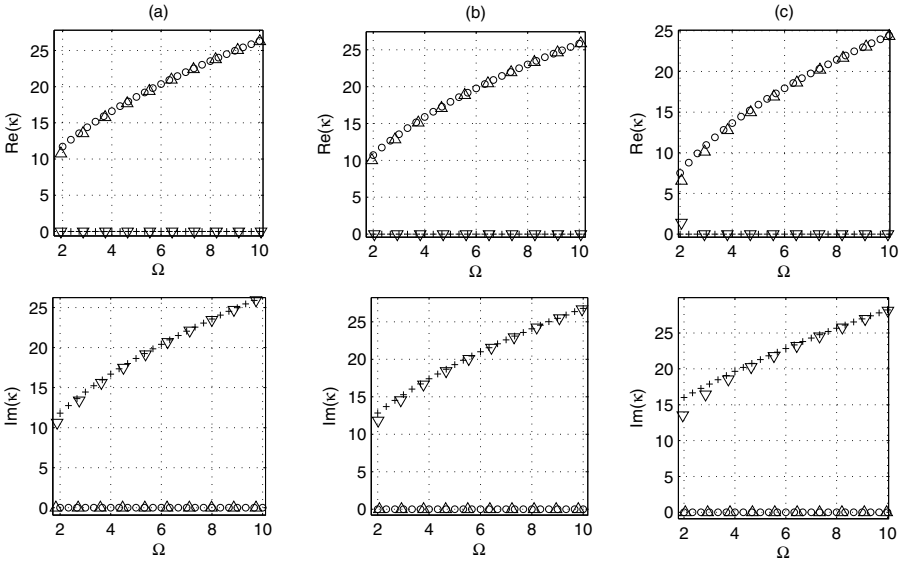

Figure 3: Comparison of the asymptotic solution for the high-frequency propagating bending wavenumber for all the theories (Eq. (5), Marker 'o') and the asymptotic solution for the high-frequency near-field bending wavenumber for all the theories (Eq. (6), Marker '+') with corresponding numerical solutions (Markers 'Δ' and '∇', respectively) - $h/a = 0.05, \nu = 0.3$, (a) $n = 1$, (b) $n = 5$, (c) $n = 10$.

where C is the correction term corresponding to the chosen theory. However, C for all the HOTs is found to be

$$C = +\frac{1}{4}\frac{n^4\left(-1+2n^2\right)}{\left(-n^2\left(-\Omega^2-n^2\Omega^2+n^6\beta^2\right)\right)^{3/4}}.$$

The near-field bending wavenumbers are as follows,

$$\kappa_{\text{nfb}} = \mathrm{i}\sqrt[4]{-n^2\left(-\Omega^2-n^2\Omega^2+n^6\beta^2\right)} + \frac{1}{4}\mathrm{i}\frac{-3\Omega^2-2n^2\Omega^2+4n^6\beta^2}{\sqrt[4]{-n^2\left(-\Omega^2-n^2\Omega^2+n^6\beta^2\right)}} + k_\beta C, \tag{9}$$

where C is the correction term corresponding to the chosen theory. Again, C remains the same for all the HOTs, given by,

$$C = +\frac{1}{4}\mathrm{i}\frac{n^4\left(-1+2n^2\right)}{\left(-n^2\left(-\Omega^2-n^2\Omega^2+n^6\beta^2\right)\right)^{3/4}}.$$

From the low-frequency expansions (Eqs. (8, 9)), it can be seen that the leading-order term ($\sqrt[4]{-n^2(-\Omega^2-n^2\Omega^2+n^6\beta^2)}$) which also appears in the denominator of the first-order correction term) goes to zero at a frequency equal to $\Omega = \frac{n^3\beta}{\sqrt{1+n^2}}$. In the vicinity of this frequency, the asymptotic expansions for the low frequency propagating and near-field bending wavenumbers are rendered invalid. Also, since the first-order correction term is proportional to n^4, this expansion breaks down for increasing n with a significant error being seen in the imaginary component of the complex wavenumber.

Fig. (4) shows a comparison of the asymptotic expression for the propagating bending wavenumber with the numerical solution (using the Flügge theory) at low frequencies for each of the four theories. Since the frequency has been scaled, one can see that the expansion becomes inaccurate progressively with frequency. Fig. (5) shows the near-field bending wavenumber at low frequencies.

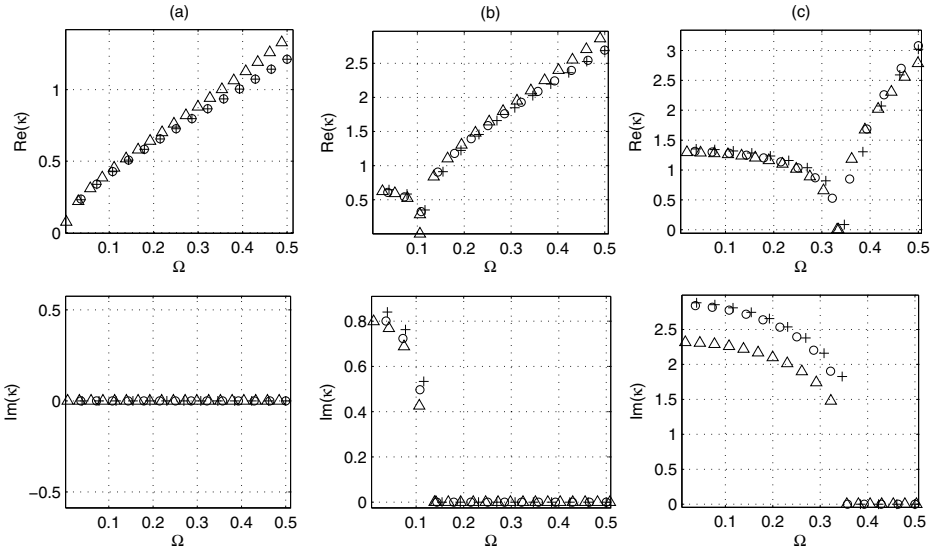

Figure 4: Comparison of the asymptotic solutions for the low-frequency propagating bending wavenumber for all the theories (Eq. (8) - Donnell-Mushtari theory (Marker '+'), Love-Timoshenko, Goldenveizer-Novozhilov, Flügge and Kennard simplified theories (Marker 'o')) - with numerical solutions for the Flügge theory (Marker 'Δ') - $h/a = 0.05, \nu = 0.3$, (a) $n = 1$, (b) $n = 3$, (c) $n = 5$.

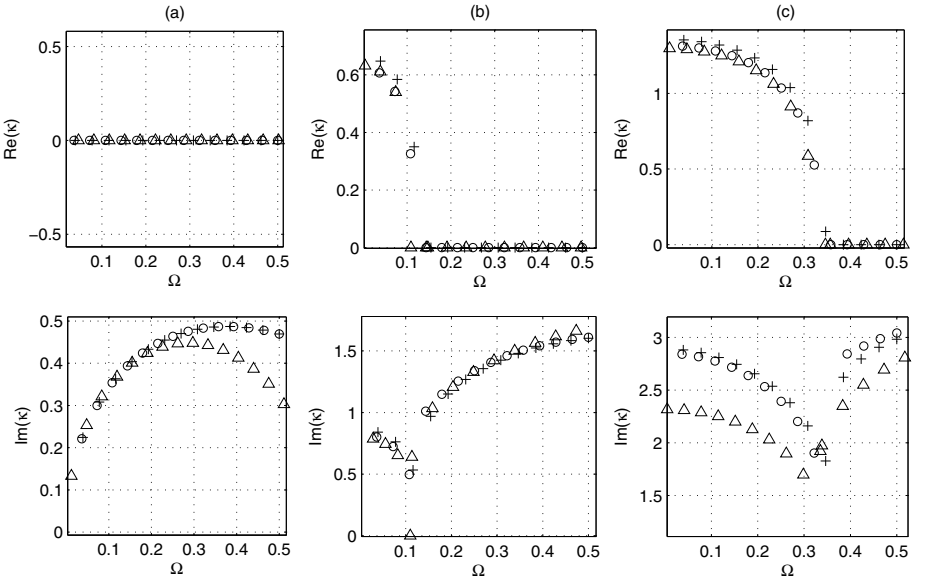

Figure 5: Comparison of the asymptotic solutions for the low-frequency near-field bending wavenumber for all the theories (Eq. (9) - Donnell-Mushtari theory (Marker '+'), Love-Timoshenko, Goldenveizer-Novozhilov, Flügge and Kennard simplified theories (Marker 'o')) - with numerical solutions for the Flügge theory (Marker 'Δ') - $h/a = 0.05, \nu = 0.3$, (a) $n = 1$, (b) $n = 3$, (c) $n = 5$.

3.4 A low-frequency expansion with an extended range of validity

The low-frequency expansions given by Eq. (8) can be seen to be rendered quickly invalid at $\Omega \approx 0.5$ with increasing n, as shown in Fig. (4). In order to improve upon this, a new expansion is chosen without making any assumption as to the magnitude of the wavenumber κ or the frequency Ω as in the previous cases of the high- and the low-frequency expansions. Also, no rescaling is applied and hence, no restrictions are placed on the nature of the relationship between κ and Ω.

Thus, we start with a simple expansion for κ of the form,

$$\kappa = \kappa_0 + \nu a_1 + \beta^2 b_1,$$

substitute this in the dispersion relation and balance the resulting equation at each

order.

$$\kappa = k_0 + \nu \frac{1}{2} \frac{(\Omega^2-1)k_0^4 + (-\Omega^4+\Omega^2+2n^2\Omega^2)k_0^2 + n^2\Omega^2(n^2+1-\Omega^2)}{k_0\left(2(\Omega^2-1)k_0^2 + 2n^2\Omega^2 - 3\Omega^4 + 3\Omega^2\right)} + ...$$
$$...\beta^2 \frac{1}{2} \frac{Nr}{k_0\left(-2k_0^2 + 2\Omega^2 k_0^2 + 2n^2\Omega^2 - 3\Omega^4 + 3\Omega^2\right)} + k_\beta C, \tag{10}$$

where,

$$Nr = k_0^8 + \left(-3\Omega^2 + 4n^2\right)k_0^6 + \left(-9n^2\Omega^2 + 6n^4 + 2\Omega^4\right)k_0^4 + ...$$
$$... \left(-9n^4\Omega^2 + 4n^2\Omega^4 + 4n^6\right)k_0^2 + 2\Omega^4 n^4 + n^8 - 3n^6\Omega^2,$$

and the leading order term in the expansion (k_0) is given by,

$$k_0 = -\frac{1}{2}\sqrt{\frac{-2\Omega\left(-3\Omega^3 + 2n^2\Omega + 3\Omega + \sqrt{\Omega^6 - 2\Omega^4 - 4n^2\Omega^2 + \Omega^2 + 4n^2 + 4n^4}\right)}{\Omega^2 - 1}}.$$

The correction terms corresponding to each of the HOTs considered are as follows,

$$C = -\frac{1}{2}\frac{Nr}{k_0\left((2\Omega^2-2)k_0^2 + 2n^2\Omega^2 - 3\Omega^4 + 3\Omega^2\right)},$$

where,

$$\begin{aligned}
Nr \text{ (LT theory)} &= \left(2\Omega^2 + 6n^2 - 2\right)k_0^4 + \left(7n^4 - 3n^2 - 3n^2\Omega^2 - 2\Omega^4 + 2\Omega^2\right)k_0^2 - ... \\
&\quad ...2n^2\Omega^4 - n^4 + 2n^6 - 3n^4\Omega^2 + 2n^2\Omega^2, \\
Nr \text{ (GN theory)} &= \left(-4\Omega^2 - 8n^2 + 4\right)k_0^4 + \left(4n^2\Omega^2 + 4\Omega^4 - 8n^4 - 4\Omega^2 + 4n^2\right)k_0^2 + ... \\
&\quad ...2n^2\Omega^4 - 2n^6 - 2n^2\Omega^2 + n^4 + 3n^4\Omega^2, \\
Nr \text{ (Flügge theory)} &= \left(4 - 3\Omega^2 - 6n^2\right)k_0^4 + \left(-8n^4 - 6\Omega^2 + 4n^2 + 10n^2\Omega^2 + 3\Omega^4\right)k_0^2 + ... \\
&\quad ...n^4 - 4n^2\Omega^2 - 3n^2\Omega^4 - 2n^6 + 5n^4\Omega^2 + 2\Omega^4, \\
Nr \text{ (KS theory)} &= \left(-2n^2 + 1\right)k_0^4 + \left(-3\Omega^2 + 6n^2\Omega^2 + 2n^2 - 4n^4\right)k_0^2 - ... \\
&\quad ...4n^2\Omega^4 + n^4 + 6\Omega^2 n^4 + 2\Omega^4 - 2n^6 - 3n^2\Omega^2.
\end{aligned}$$

'LT' stands for Love-Timoshenko, 'GN' stands for Goldenveizer-Novozhilov and 'KS' stands for Kennard-simplified theories, respectively.

In comparison with Eq. (8) (plotted in Fig. (4)), Eq. (10) is valid above the cut-on frequency beyond which the flexural wavenumber is purely real and is plotted in Fig. (6) in this frequency range for a range of n values. The different theories are denoted by different markers (explained in the figure caption) and compared with a numerical solution based on the Flügge theory in each case.

The improvement in accuracy is significant for lower values of n. At $n = 3$, this improvement is marginal, as can be seen when compared with Fig. (4).

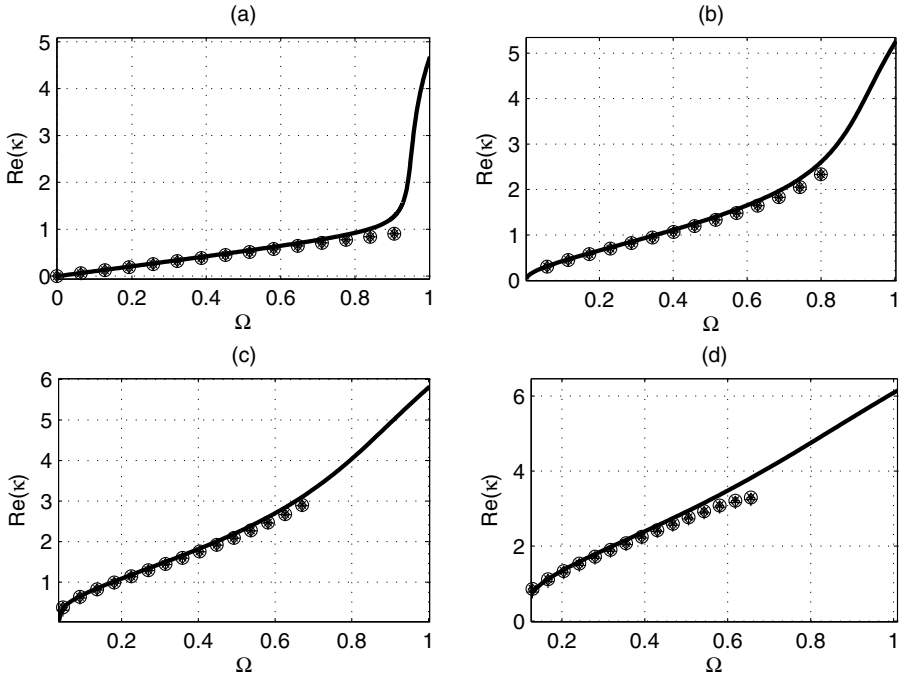

Figure 6: Comparison of the asymptotic solutions for the intermediate-frequency flexural wavenumber for all the theories (Eq. (10)) - Donnell-Mushtari theory (Marker '+'), Love-Timoshenko theory (Marker 'o'), Goldenveizer-Novozhilov theory (Marker '$\times$'), Flügge theory (Marker '$*$') and Kennard simplified theory (Marker '$\diamond$') - with numerical solutions for the Flügge theory (Marker '–') - $h/a = 0.05, \nu = 0.3$, (a) $n = 0$, (b) $n = 1$, (c) $n = 2$, (d) $n = 3$.

3.5 Flexural wavenumber ($n = 1$) : very low frequency behaviour of DM theory

Fig. (7) shows the numerical solutions of the dispersion relation for $n = 1$ for the various shell theories for a very low frequency value ($\Omega = 0.01 - 0.05$). From the figure, it can be seen that at very low frequency, the error in the DM theory is significant when compared with the Goldenveizer-Novozhilov theory and the Flügge theory. The wavenumber obtained from the DM theory goes to zero at $\Omega \approx 0.01$ and becomes complex-valued below this. In actuality, the wavenumber remains purely real till $\Omega = 0$, as reflected by the Goldenveizer-Novozhilov and Flügge theories. The frequency range over which this error is significant is, however, very small when compared with the frequency range that has been covered by the wavenumber expansions presented in this paper.

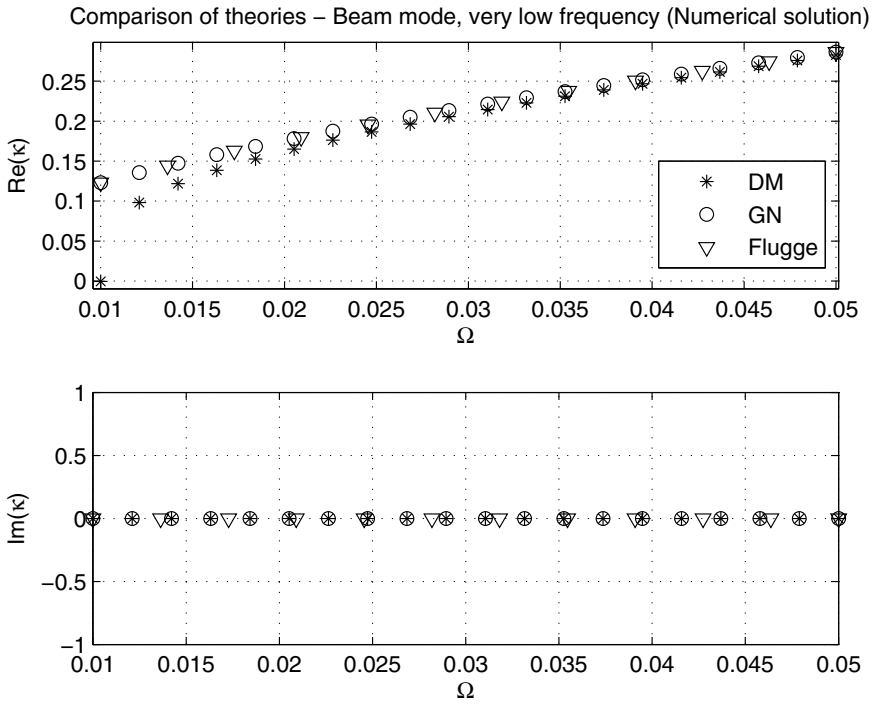

Figure 7: Comparison of Donnell-Mushtari (DM), Goldenveizer-Novozhilov(GN) and Flügge theories - Very low frequency *in vacuo* isotropic propagating bending wavenumber, beam mode ($n = 1$) - Comparison of numerical solutions - $\nu = 0.3$, $\beta = 0.05/\sqrt{12}$

3.6 High-frequency longitudinal and torsional wavenumbers : $n \geq 1$

The high-frequency longitudinal and torsional wavenumbers are obtained by using the scaling transformation,

$$\kappa = \frac{\kappa_{rs}}{\eta}, \; \Omega = \frac{\Omega_{rs}}{\eta}. \tag{11}$$

Thus, using this to rescale the dispersion relation and using a perturbation expansion for κ_{rs} of the form $\kappa_{rs} = \kappa_0 + \eta a_1 + k_\beta b_1 + \nu c_1 + \eta^2 d_1 + k_\beta^2 e_1 + \nu^2 f_1$, the dispersion relation is balanced at each order to yield the solution for the wavenumber.

3.6.1 Longitudinal wavenumbers

The asymptotic expansion for the longitudinal wavenumber for each of the theories, in the unscaled variables is given by

$$\kappa_{\text{long}} = \Omega - \frac{1}{2}\frac{n^2}{\Omega} + C, \tag{12}$$

where κ_{long} is the longitudinal wavenumber. The correction term C for each of the HOTs is found to be zero except in the case of the Flügge theory. Here,

$$C \text{ (Flügge theory)} = \frac{1}{2}k_\beta^2\frac{\Omega}{\beta^2}.$$

It is interesting to note that even though the correction term appears to be $\mathcal{O}(k_\beta^2)$, it actually is of $\mathcal{O}(k_\beta^2/\beta^2) = \mathcal{O}(k_\beta)$, since $k_\beta = \beta^2$ by definition.

Fig. (8) shows the comparison between the asymptotic expansions for the longitudinal wavenumbers with the numerical solution for the Flügge theory.

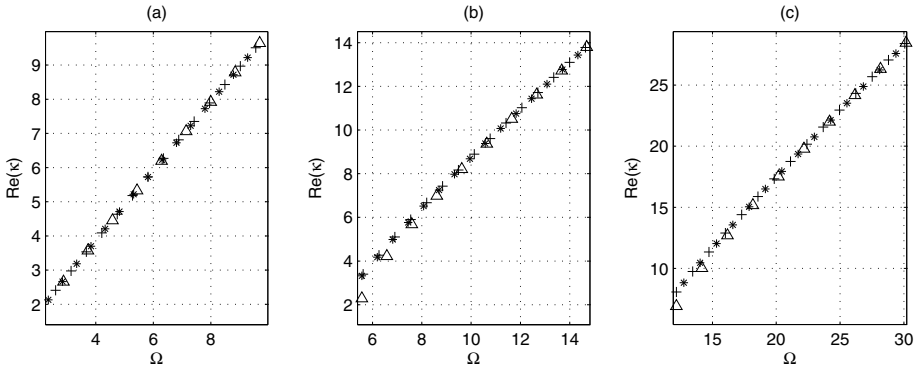

Figure 8: Comparison of the asymptotic solutions for the high-frequency longitudinal wavenumber for the Donnell-Mushtari, Love-Timoshenko, Goldenveizer-Novozhilov and Kennard-simplifed theories (Marker '+') and the Flügge theory (Marker '$*$') (Eq. (12)) with numerical solutions for the Flügge theory (Marker 'Δ') - $h/a = 0.05, \nu = 0.3$, (a) $n = 1$, (b) $n = 5$, (c) $n = 10$.

3.6.2 Torsional wavenumbers

For the torsional wavenumber, however, the difference between the HOTs and the Donnell-Mushtari theory is a first-order term. Thus, the asymptotic expansions for the torsional wavenumbers corresponding to each shell theory are shown below.

$$\kappa_{\text{tors}} = \sqrt{2}\Omega + \frac{1}{2}\nu\sqrt{2}\Omega - \frac{1}{4}\frac{n^2\sqrt{2}}{\Omega} + \frac{3}{8}\nu^2\sqrt{2}\Omega + C, \tag{13}$$

where,

$$\begin{aligned} C \text{ (Love-Timoshenko theory)} &= -k_\beta\sqrt{2}\Omega + \frac{3}{2}k_\beta^2\sqrt{2}\Omega, \\ C \text{ (Goldenveizer-Novozhilov theory)} &= -2k_\beta\sqrt{2}\Omega + 6k_\beta^2\sqrt{2}\Omega, \\ C \text{ (Flügge theory)} &= -\frac{3}{2}k_\beta\sqrt{2}\Omega + \frac{27}{8}k_\beta^2\sqrt{2}\Omega, \\ C \text{ (Kennard-simplified theory)} &= 0. \end{aligned}$$

Fig. (9) shows the comparison between the asymptotic expansions for the torsional wavenumbers with the numerical solution for the Flügge theory.

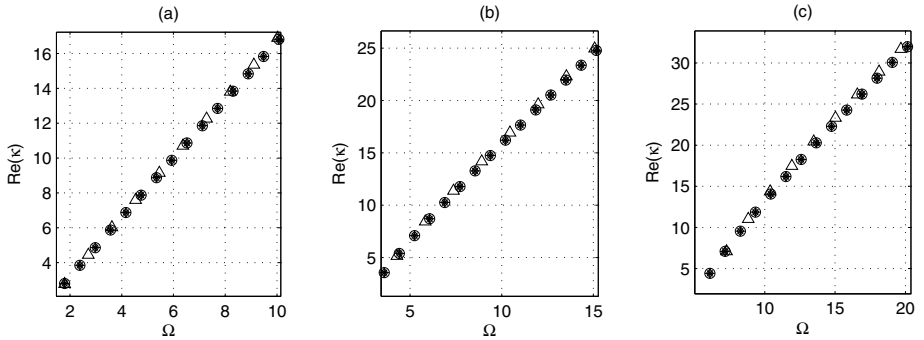

Figure 9: Comparison of the asymptotic solutions for the high-frequency torsional wavenumber for all the theories (Eq. (13)) - Donnell-Mushtari theory (Marker '+'), Love-Timoshenko theory (Marker 'o'), Goldenveizer-Novozhilov theory (Marker '×'), Flügge theory (Marker '∗') and Kennard simplified theory (Marker '◇') - with numerical solutions for the Flügge theory (Marker 'Δ') - $h/a = 0.05, \nu = 0.3$, (a) $n = 1$, (b) $n = 5$, (c) $n = 10$.

The longitudinal and torsional wavenumbers do not cut on at very low frequencies and so, they cannot be found via a regular perturbation approach.

4 Fluid-filled infinite shell

The equations of motion for a fluid-filled shell are obtained by substituting for the fluid-loading term $\mathscr{F}$ as $\mathscr{F} = -\mu\Omega^2\frac{J_n(\xi)}{\xi J_n'(\xi)}$ in Eq. (2) [Sarkar and Sonti (2007b);

Fuller (1983)]. μ is the fluid-loading parameter given by $\mu = \frac{\rho_f a}{\rho_s h}$, where ρ_f is the density of the fluid. ξ is the radial wavenumber given by $\xi = \sqrt{c^2\Omega^2 - \kappa^2}$, where $c = c_L/c_f$. c_L is as defined earlier and c_f is the speed of sound in a quiescent fluid. The determinant of this matrix, when equated to zero, gives the coupled dispersion relation.

The solutions to the dispersion relation in this section are obtained for the two cases of $\mu \ll 1$ and $\mu \gg 1$. These cases correspond to light and heavy fluid-loading, respectively. The limiting cases of $\mu = 0$ and $\mu = \infty$ correspond to the cases of a rigid-walled duct and a pressure-release duct, respectively.

Figures (10, 11) present a schematic of the wavenumbers for the small μ and the large μ cases, respectively, for both isotropic and orthotropic shells. $S = 0$ represents the *in vacuo* bending wavenumber, $R = 0$ corresponds to the uncoupled rigid-duct cut-on and $PR = 0$ corresponds to the uncoupled pressure-release cut-on. The coupled wavenumbers which are found in the following sections are perturbations to these uncoupled wavenumbers.

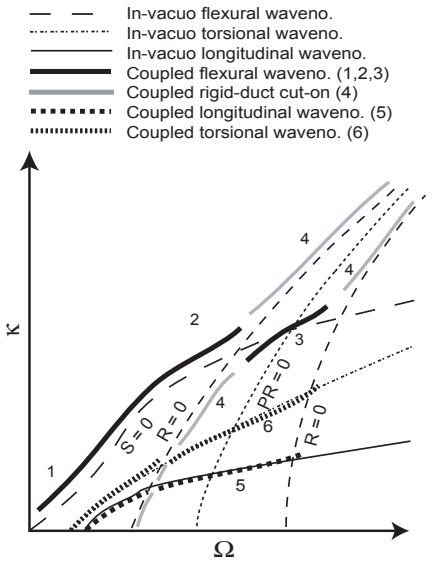

Figure 10: Schematic of coupled wavenumbers - Small μ.

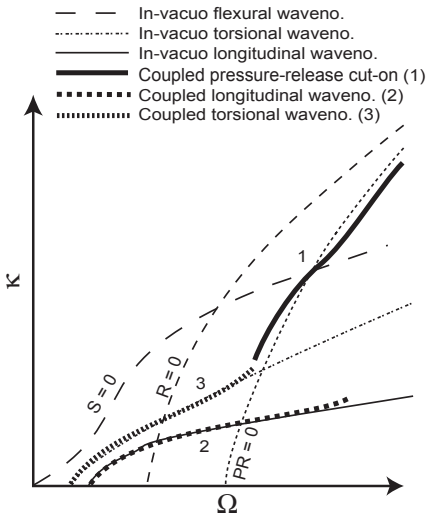

Figure 11: Schematic of coupled wavenumbers - Large μ.

4.1 Light fluid loading : $\mu \ll 1$

4.1.1 Coupled rigid-duct cut-on wavenumber

The coupled rigid-duct (RD) cut-on is a perturbation to the uncoupled RD cut-on wavenumber. The asymptotic expansion for this wavenumber is found by substituting $\kappa = \kappa_0 + \mu a_1 + \nu b_1 + k_\beta c_1$ in the coupled dispersion relation. This is now balanced at orders to yield the final solution for κ. This is given by

$$\kappa = \kappa_0 - \mu \frac{\xi_0^2 \Omega^2 Nr}{\kappa_0 (n^2 - \xi_0^2) Dr} + k_\beta C, \tag{14}$$

where,

$$\begin{aligned} Nr =& \left(\kappa_0^4 + \left(-3\Omega^2 + 2n^2\right)\kappa_0^2 + \left(2\Omega^4 - 3\Omega^2 n^2 + n^4\right)\right), \\ Dr =& \kappa_0^8 \beta^2 + \left(4\beta^2 n^2 - 3\Omega^2 \beta^2\right)\kappa_0^6 + ... \\ & \left(2\Omega^4 \beta^2 - 9\Omega^2 \beta^2 n^2 + 1 - \Omega^2 + 6\beta^2 n^4\right)\kappa_0^4 + ... \\ & \left(3\Omega^4 + 4\Omega^4 \beta^2 n^2 - 3\Omega^2 - 2\Omega^2 n^2 - 9\Omega^2 \beta^2 n^4 + 4n^6 \beta^2\right)\kappa_0^2 + ... \\ & \left(-2\Omega^6 + 3n^2\Omega^4 + 2\Omega^4 \beta^2 n^4 + 2\Omega^4 + n^8 \beta^2 - \Omega^2 n^4 - \Omega^2 n^2 - 3n^6 \Omega^2 \beta^2\right). \end{aligned}$$

Here, κ_0 is given by the solution of $J_n'(\xi_0) = J_n'\left(\sqrt{c^2\Omega^2 - \kappa_0^2}\right) = 0$. The value of C was found to be zero for all the HOTs.

Fig. (12) shows a comparison of the asymptotic expression for the coupled RD cut-on wavenumber with the numerical solution (using the Flügge theory) for each of the theories.

4.1.2 Coupled structural wavenumbers : High frequency ($\mu \ll 1$)

It is difficult to obtain an expansion for κ by rescaling the wavenumber κ and frequency Ω with a fictitious parameter η and using a series expansion of the form $\kappa = \kappa_0 + \eta a_1 + \mu b_1 + \nu c_1 + k_\beta d_1$. Thus, we employ a two-step expansion method [Kunte, Sarkar, and Sonti (2010)].

In the first step, κ is expanded as $\kappa = \kappa_0 + \mu a_1 + k_\beta b_1$. This is substituted in the coupled dispersion relation and the resulting expression is balanced at each order. This results in a complicated expression at $\mathscr{O}(1)$ which can be solved to obtain an expression for κ_0. This step is however delayed till a later stage. Balancing at subsequent orders allows us to find these coefficients as a function of κ_0. The $\mathscr{O}(1)$ equation is now solved asymptotically rather than exactly, by rescaling κ_0 and Ω suitably, depending on the frequency range and the nature of the wavenumber to be studied. This method is based on the fact that the leading-order term is the

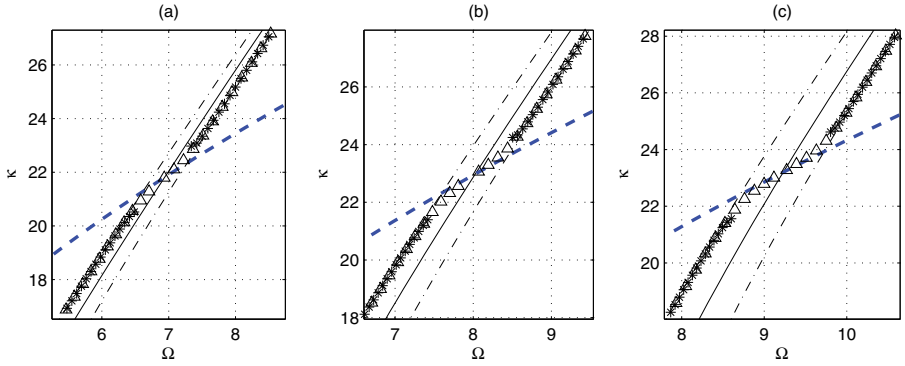

Figure 12: Comparison of asymptotic solution for the coupled RD cut-on wavenumber for all the theories (Section 4 in Fig. (10)) (Eq. (14), Marker '$*$') with the corresponding numerical solution using the Flügge theory (Marker 'Δ') - $h/a = 0.05, \nu = 0.3, \mu = 0.2564, c = 3.4673$, (a) $n = 1$, (b) $n = 5$, (c) $n = 10$. (Also shown are the *in vacuo* flexural wavenumber (Marker '- -'), the uncoupled PR cut-on wavenumber (Marker '—') and the uncoupled RD cut-on wavenumber (Marker '-.-').)

dominant term in an asymptotic expansion and the method has been shown to work well by Kunte, Sarkar, and Sonti (2010). Thus, the asymptotic expansion obtained for κ (in terms of the leading order solution κ_0) is of the form,

$$\kappa = \kappa_0 + \mu \frac{1}{2}\frac{N}{D}\frac{\Omega^2 J_n(\xi_0)}{\kappa_0 \xi_0 J_n'(\xi_0)} + k_\beta C, \tag{15}$$

where,

$$\begin{aligned}
N =& ((\nu-1)\kappa_0^4 + ((2n^2-\Omega^2)\nu + 3\Omega^2 - 2n^2)\kappa_0^2 + (-n^2\Omega^2 + n^4)\nu + 3n^2\Omega^2 - 2\Omega^4 - n^4),\\
D =& ((4\beta^2\nu - 4\beta^2)\kappa_0^6 + (9\Omega^2\beta^2 - 12\beta^2 n^2 + (-3\Omega^2\beta^2 + 12\beta^2 n^2)\nu)\kappa_0^4 + \ldots\\
& (-2\nu^3 + (12\beta^2 n^4 + 2 - 2\Omega^2 - 6\Omega^2\beta^2 n^2)\nu + 18\Omega^2\beta^2 n^2 + \ldots\\
& 2\nu^2 - 4\Omega^4\beta^2 + 2\Omega^2 - 2 - 12\beta^2 n^4)\kappa_0^2 + \ldots\\
& 9\Omega^2\beta^2 n^4 - 2\nu^2\Omega^2 - 3\Omega^4 + (\Omega^4 - 2n^2\Omega^2 - \Omega^2 + 4n^6\beta^2 - 3\Omega^2\beta^2 n^4)\nu - \ldots\\
& 4n^6\beta^2 - 4\Omega^4\beta^2 n^2 + 3\Omega^2 + 2n^2\Omega^2).
\end{aligned}$$

Before presenting the correction term C for each of the HOTs, we make a few remarks on the leading-order term κ_0 in the expansion. The expression for κ_0 is found by rescaling the $\mathscr{O}(1)$ equation and expanding the rescaled leading-order term as

in the previous section for an *in vacuo* shell. The leading order solutions for the high-frequency bending, low-frequency bending and high-frequency longitudinal and torsional wavenumbers are identical to those for the *in vacuo* shell given by Eqs. (5, 6), Eqs.(8, 9) and Eqs.(12, 13), respectively, after setting $k_\beta = 0$ (since k_β is used as an asymptotic expansion parameter at the first stage to yield the solution in Eq. (15)).

The leading-order solutions (for κ_0) are repeated here for convenience. Since our primary interest lies in noise generation, only the real wavenumbers (which occur at high frequencies) will be listed here and also plotted subsequently. Also, since we wish to study the effect of the fluid-loading and the differences in the various shell theories with fluid-loading, for the moment we ignore the higher order terms in ν while solving for the leading-order term, ensuring at the same time that the accuracy of the resultant expression is not harmed. These high frequency wavenumbers are,

$$\kappa_{\text{flex,prop}} = \sqrt{\frac{\Omega}{\beta}} - \frac{1}{2}\frac{n^2}{\sqrt{\frac{\Omega}{\beta}}}, \tag{16}$$

$$\kappa_{\text{long}} = \Omega - \frac{1}{2}\frac{n^2}{\Omega}, \tag{17}$$

$$\kappa_{\text{tors}} = \sqrt{2}\Omega - \frac{1}{2}\frac{n^2}{\sqrt{2}\Omega} + \frac{1}{2}\nu\sqrt{2}\Omega, \tag{18}$$

where $\kappa_{\text{flex,prop}}$ is the propagating flexural wavenumber, κ_{long} is the longitudinal wavenumber and κ_{tors} is the torsional wavenumber.

The term C is given below for each of the HOTs.

$$C \text{ (Love-Timoshenko theory)} = -\frac{1}{2}\frac{Nr}{\kappa_0 Dr},$$

where,

$$
\begin{aligned}
Nr =&(-2\beta^2+2\beta^2\nu)\kappa_0^8+(-\nu^2n^2\beta^2+(6\beta^2n^2-2\Omega^2\beta^2)\nu-7\beta^2n^2+2\Omega^2\beta^2)\kappa_0^6+...\\
&(6n^2-9\beta^2n^4+6\Omega^2\beta^2n^2+2\Omega^2-2+(n^2-2)\nu^3+(2-2\beta^2n^4-2n^2)\nu^2+...\\
&(7\beta^2n^4+2-4\Omega^2\beta^2n^2-5n^2-2\Omega^2)\nu)\kappa_0^4+...\\
&(6\Omega^2\beta^2n^4-3n^2-2\Omega^4+7n^4-5n^6\beta^2-3n^2\Omega^2+2\Omega^2+(-n^6\beta^2-n^4+...\\
&n^2\Omega^2+n^2)\nu^2+(2\Omega^4+2n^2-2\Omega^2-2\Omega^2\beta^2n^4-6n^4+4n^6\beta^2)\nu)\kappa_0^2+...\\
&((n^4-2n^6+n^8\beta^2-\Omega^2n^4)\nu+2n^2\Omega^2+2n^6-3\Omega^2n^4+...\\
&2n^6\Omega^2\beta^2-n^4-n^8\beta^2-2n^2\Omega^4),\\
Dr =&(4\beta^2\nu-4\beta^2)\kappa_0^6+(9\Omega^2\beta^2-12\beta^2n^2+(-3\Omega^2\beta^2+12\beta^2n^2)\nu)\kappa_0^4+...\\
&(-2\nu^3+(12\beta^2n^4+2-2\Omega^2-6\Omega^2\beta^2n^2)\nu+18\Omega^2\beta^2n^2+2\nu^2-4\Omega^4\beta^2+...\\
&2\Omega^2-2-12\beta^2n^4)\kappa_0^2+9\Omega^2\beta^2n^4-2\nu^2\Omega^2-3\Omega^4+(\Omega^4-2n^2\Omega^2-...\\
&\Omega^2+4n^6\beta^2-3\Omega^2\beta^2n^4)\nu-4n^6\beta^2-4\Omega^4\beta^2n^2+3\Omega^2+2n^2\Omega^2
\end{aligned}
$$

$$
C\text{ (Goldenveizer-Novozhilov theory) } = -\frac{1}{2}\frac{Nr}{\kappa_0 Dr},
$$

where,

$$
\begin{aligned}
Nr =&(-4\beta^2+4\beta^2\nu)\kappa_0^8+(-2\nu^2n^2\beta^2+(-4\Omega^2\beta^2+12\beta^2n^2)\nu-12\beta^2n^2+4\Omega^2\beta^2)\kappa_0^6...\\
&+(-4+4\Omega^2+(4-4\beta^2n^4-2n^2)\nu^2-13\beta^2n^4+(-4\Omega^2+4-...\\
&8\Omega^2\beta^2n^2-8n^2+13\beta^2n^4)\nu+10\Omega^2\beta^2n^2+8n^2+(2n^2-4)\nu^3)\kappa_0^4+...\\
&(-4\Omega^2n^2+4\Omega^2-4n^2+8\Omega^2\beta^2n^4-6n^6\beta^2+(2\Omega^2n^2-2n^6\beta^2)\nu^2-...\\
&4\Omega^4+(4\Omega^4-4\Omega^2-8n^4+4n^2+6n^6\beta^2-4\Omega^2\beta^2n^4)\nu+8n^4)\kappa_0^2+...\\
&(-n^4-n^8\beta^2+2\Omega^2n^6\beta^2-2n^2\Omega^4-3\Omega^2n^4+...\\
&(n^8\beta^2-2n^6+n^4-\Omega^2n^4)\nu+2n^6+2\Omega^2n^2),\\
Dr =&(-4\beta^2+4\beta^2\nu)\kappa_0^6+(9\Omega^2\beta^2+(12\beta^2n^2-3\Omega^2\beta^2)\nu-12\beta^2n^2)\kappa_0^4+...\\
&(18\Omega^2\beta^2n^2-2-12\beta^2n^4-2\nu^3+2\Omega^2+2\nu^2+...\\
&(-6\Omega^2\beta^2n^2-2\Omega^2+2+12\beta^2n^4)\nu-4\Omega^4\beta^2)\kappa_0^2+...\\
&(-4n^6\beta^2-2\nu^2\Omega^2-4\Omega^4\beta^2n^2+(4n^6\beta^2-3\Omega^2\beta^2n^4-\Omega^2+\Omega^4-2\Omega^2n^2)\nu-...\\
&3\Omega^4+9\Omega^2\beta^2n^4+3\Omega^2+2\Omega^2n^2).
\end{aligned}
$$

$$
C\text{ (Flügge theory) } = -\frac{1}{2}\frac{Nr}{\kappa_0 Dr},
$$

where,

$$
\begin{aligned}
Nr =&(-3\beta^2+3\nu\beta^2)\kappa_0^8+...\\
&((2-3\Omega^2\beta^2+10\beta^2n^2)\nu+(-2\beta^2n^2-2)\nu^2-8\beta^2n^2+3\Omega^2\beta^2)\kappa_0^6+...\\
&(-3\nu^3-(-3+4\beta^2n^4)\nu^2-(-4+6n^2+7\Omega^2\beta^2n^2+7\Omega^2-12\beta^2n^4)\nu...\\
&-4+3\Omega^2-8\beta^2n^4+6n^2+7\Omega^2\beta^2n^2)\kappa_0^4+...\\
&(5\Omega^2\beta^2n^4-3\Omega^4-4n^6\beta^2+6\Omega^2+8n^4-4n^2-10n^2\Omega^2+(-2n^2+2n^4-...\\
&2n^6\beta^2)\nu^2+(3\Omega^4-5\Omega^2\beta^2n^4-10n^4+6n^6\beta^2-4\Omega^2+2n^2\Omega^2+6n^2)\nu)\kappa_0^2+...\\
&((-2n^6+n^4+n^4\Omega^2-2n^2\Omega^2-n^6\Omega^2\beta^2+n^8\beta^2+n^2\Omega^4)\nu-...\\
&2\Omega^4+4n^2\Omega^2-n^8\beta^2+2n^6-n^4+3n^2\Omega^4-5n^4\Omega^2+n^6\Omega^2\beta^2),\\
Dr =&(-4\beta^2+4\nu\beta^2)\kappa_0^6+((12\beta^2n^2-3\Omega^2\beta^2)\nu+9\Omega^2\beta^2-12\beta^2n^2)\kappa_0^4+...\\
&(-2-12\beta^2n^4-4\Omega^4\beta^2+2\Omega^2-2\nu^3+18\Omega^2\beta^2n^2+2\nu^2+...\\
&(2+12\beta^2n^4-6\Omega^2\beta^2n^2-2\Omega^2)\nu)\kappa_0^2+...\\
&(2n^2\Omega^2-2\nu^2\Omega^2-4n^6\beta^2+(-3\Omega^2\beta^2n^4+\Omega^4-2n^2\Omega^2-\Omega^2+4n^6\beta^2)\nu+...\\
&9\Omega^2\beta^2n^4+3\Omega^2-4\Omega^4\beta^2n^2-3\Omega^4).
\end{aligned}
$$

Finally,

$$C\text{ (Kennard-simplified theory)} = \frac{1}{4}\frac{Nr}{\kappa_0 Dr},$$

where,

$$
\begin{aligned}
Nr =&((-5n^2+1)\nu-2+(1+n^2)\nu^2+4n^2)\kappa_0^4+...\\
&(-12n^2\Omega^2+(-16n^4+7n^2\Omega^2+8n^2+\Omega^2)\nu+(-n^2\Omega^2+5n^4-\Omega^2-n^2)\nu^2-...\\
&4n^2+(3n^4-3n^2)\nu^3+8n^4+6\Omega^2)\kappa_0^2+...\\
&((4n^6-2n^4-n^4\Omega^2-n^2\Omega^2)\nu^2+(-8n^6+4n^4-5n^2\Omega^2-2n^2\Omega^4+...\\
&13n^4\Omega^2-2\Omega^4)\nu+6n^2\Omega^2+8n^2\Omega^4-4\Omega^4-2n^4-12n^4\Omega^2+4n^6),\\
Dr =&(4\beta^2\nu^2-8\beta^2\nu+4\beta^2)\kappa_0^6+(12\beta^2n^2+(-3\beta^2\Omega^2+12\beta^2n^2)\nu^2-9\beta^2\Omega^2+...\\
&(12\beta^2\Omega^2-24\beta^2n^2)\nu)\kappa_0^4+...\\
&(-2\nu^4-2\Omega^2+4\Omega^4\beta^2+(-24\beta^2n^4+24\beta^2\Omega^2n^2+4\Omega^2-4\Omega^4\beta^2-4)\nu+...\\
&(-6\beta^2\Omega^2n^2+12\beta^2n^4-2\Omega^2)\nu^2+2+4\nu^3-18\beta^2\Omega^2n^2+12\beta^2n^4)\kappa_0^2+...\\
&((\Omega^2-3\beta^2\Omega^2n^4-2n^2\Omega^2+4n^6\beta^2+\Omega^4)\nu^2+...\\
&(-4\Omega^4-4\Omega^4\beta^2n^2+12\beta^2\Omega^2n^4-8n^6\beta^2+4n^2\Omega^2+4\Omega^2)\nu)-...\\
&2n^2\Omega^2-2\nu^3\Omega^2+4\Omega^4\beta^2n^2+3\Omega^4-9\beta^2\Omega^2n^4+4n^6\beta^2-3\Omega^2.
\end{aligned}
$$

Fig. (13) shows a comparison of the asymptotic expression for the high-frequency coupled flexural wavenumber at a frequency below the first RD coincidence frequency along with the numerical solution (using the Flügge theory) for each of the five theories. Fig. (14) shows a comparison of the asymptotic expression for the

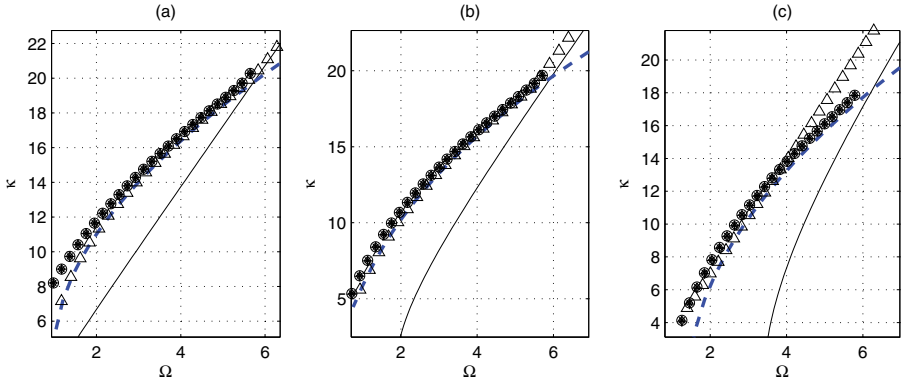

Figure 13: Comparison of asymptotic solution for the coupled flexural wavenumber (high-frequency, below the first coincidence) for all the theories (Section 2 in Fig. (10)) (Eqs. (15, 16)) - Donnell-Mushtari theory (Marker '+'), Love-Timoshenko theory (Marker 'o'), Goldenveizer-Novozhilov theory (Marker '$\times$'), Flügge theory (Marker '$*$') and Kennard simplified theory (Marker '$\diamond$') - with numerical solutions for the Flügge theory (Marker 'Δ') - $h/a = 0.05, \nu = 0.3, \mu = 0.2564, c = 3.4673$, (a) $n = 1$, (b) $n = 5$, (c) $n = 10$. (Also shown are the *in vacuo* flexural wavenumber (Marker '- -') and the first uncoupled RD cut-on wavenumber (Marker '—').)

high-frequency coupled flexural wavenumber at an uncoupled PR coincidence frequency along with the numerical solution (using the Flügge theory) for each of the five theories. Fig. (15) shows a comparison of the asymptotic expression for the coupled longitudinal wavenumber with the numerical solution (using the Flügge theory) and Fig. (16) shows a comparison of the asymptotic expression for the coupled torsional wavenumber with the numerical solution (using the Flügge theory) for each of the five theories.

As can be seen from the schematic figure for the small μ case (Fig. (10)) and Eq. (15), the coupled longitudinal and coupled torsional wavenumbers also show a similar behaviour as the coupled flexural wavenumber, i.e., the coupled structural wavenumber expansion is invalid in the vicinity of the coincidence frequencies. However, this effect is not as dramatic as in the case of the coupled flexural wavenumber and hence, it appears as a single continuous curve in the figures. Zooming in very close to the coincidence frequency reveals a similar 'gap' effect

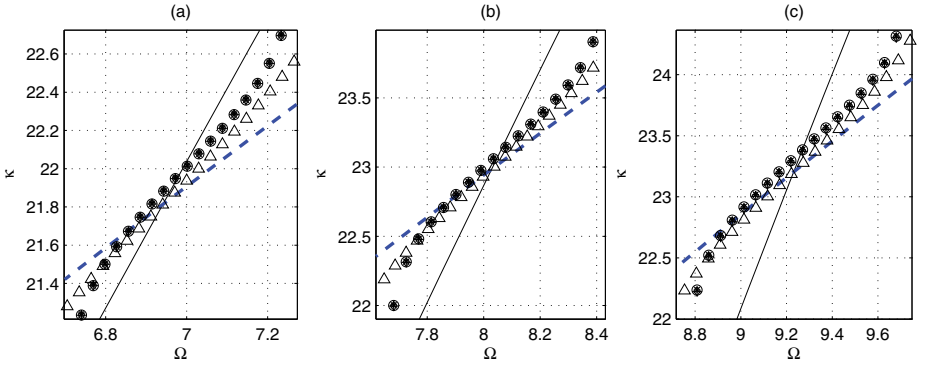

Figure 14: Comparison of asymptotic solution for the coupled flexural wavenumber (high-frequency, at an uncoupled PR coincidence) for all the theories (Section 3 in Fig. (10)) (Eqs. (15, 16)) - Donnell-Mushtari theory (Marker '+'), Love-Timoshenko theory (Marker 'o'), Goldenveizer-Novozhilov theory (Marker '×'), Flügge theory (Marker '∗') and Kennard simplified theory (Marker '⋄') - with numerical solutions for the Flügge theory (Marker 'Δ') - $h/a = 0.05, \nu = 0.3, \mu = 0.2564, c = 3.4673$, (a) $n = 1$, (b) $n = 5$, (c) $n = 10$. (Also shown are the *in vacuo* flexural wavenumber (Marker '- -') and the uncoupled PR cut-on wavenumber (Marker '—').)

as has been noted previously by Sarkar and Sonti (2007a,b).

4.2 Heavy fluid loading : $\mu \gg 1$

4.2.1 Coupled pressure-release cut-on wavenumber

The coupled pressure-release (PR) cut-on wavenumber is a perturbation to the uncoupled PR cut-on wavenumber. In order to use a regular perturbation expansion, we substitute $\mu = 1/\varepsilon$ in the coupled dispersion relation. Now, $\varepsilon \ll 1$. The wavenumber κ can now be expanded in an asymptotic series of the form $\kappa = \kappa_0 + \varepsilon a_1 + \nu b_1 + k_\beta c_1$. Balancing the coupled dispersion relation at each order, the final solution for the wavenumber is obtained. This is given by

$$\kappa = \kappa_0 - \frac{1}{\mu} \frac{\xi_0^2 Nr}{\kappa_0 \Omega^2 Dr} + k_\beta C, \tag{19}$$

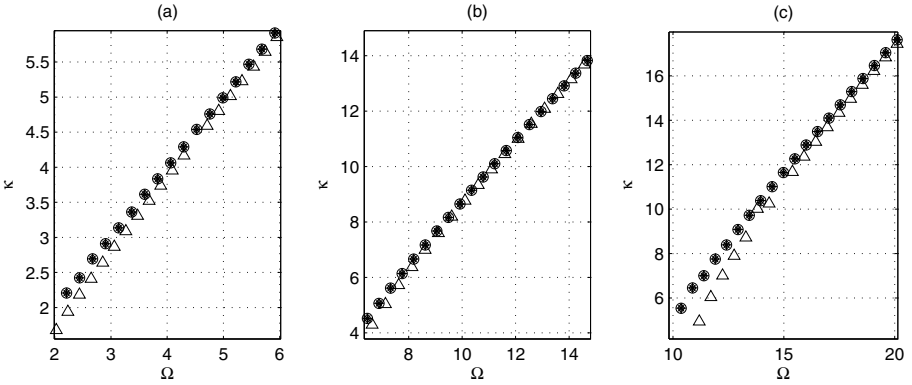

Figure 15: Comparison of asymptotic solution for the coupled longitudinal wavenumber (small μ) for all the theories (Section 5 in Fig. (10)) (Eqs. (15, 17)) - Donnell-Mushtari theory (Marker '+'), Love-Timoshenko theory (Marker 'o'), Goldenveizer-Novozhilov theory (Marker '$\times$'), Flügge theory (Marker '$*$') and Kennard simplified theory (Marker '$\diamond$') - with the corresponding numerical solution using the Flügge theory (Marker 'Δ') - $h/a = 0.05, \nu = 0.3, \mu = 0.2564, c = 3.4673$, (a) $n = 1$, (b) $n = 5$, (c) $n = 10$.

where,

$$\begin{aligned} Nr =& \beta^2\kappa_0^8 + \left(-3\beta^2\Omega^2 + 4\beta^2 n^2\right)\kappa_0^6 + \ldots \\ & (6n^4\beta^2 + 2\beta^2\Omega^4 - \Omega^2 + 1 - 9\Omega^2\beta^2 n^2)\kappa_0^4 + \ldots \\ & (4n^6\beta^2 + 4\beta^2 n^2\Omega^4 - 9n^4\beta^2\Omega^2 + 3\Omega^4 - 2\Omega^2 n^2 - 3\Omega^2)\kappa_0^2 + \ldots \\ & (-\Omega^2 n^2 - n^4\Omega^2 - 2\Omega^6 + 3\Omega^4 n^2 + 2\Omega^4 + 2n^4\beta^2\Omega^4 - 3\Omega^2 n^6\beta^2 + n^8\beta^2), \end{aligned} \tag{20}$$

$$Dr = \left(\kappa_0^4 + \left(-3\Omega^2 + 2n^2\right)\kappa_0^2 + 2\Omega^4 - 3\Omega^2 n^2 + n^4\right). \tag{21}$$

κ_0 is given by the solution of $J_n(\xi_0) = J_n\left(\sqrt{c^2\Omega^2 - \kappa_0^2}\right) = 0$. As in the case of the coupled RD cut-ons, the correction term C goes to zero for all of the theories, implying that this is a higher-order effect.

Fig. (17) shows a comparison of the asymptotic expression for the coupled PR cut-on wavenumber with the numerical solution (using the Flügge theory) for each of the four theories. The density of the fluid is chosen to be $\rho_f = 2000\text{kg/m}^3$, while speed of sound in the fluid is kept at $c_f = 1500\text{m/s}$. These physical values result in the following non-dimensional parameter values, $\mu = 5.1282, c = 3.4673$, which can be conveniently studied using asymptotic methods.

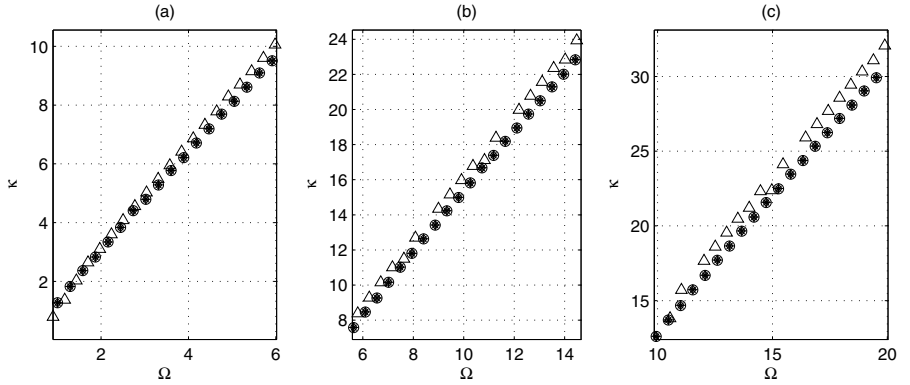

Figure 16: Comparison of asymptotic solution for the coupled torsional wavenumber (small μ) for all the theories (Section 6 in Fig. (10)) (Eqs. (15, 18)) - Donnell-Mushtari theory (Marker '+'), Love-Timoshenko theory (Marker 'o'), Goldenveizer-Novozhilov theory (Marker '$\times$'), Flügge theory (Marker '$*$') and Kennard simplified theory (Marker '$\diamond$') - with the corresponding numerical solution using the Flügge theory (Marker 'Δ') - $h/a = 0.05, \nu = 0.3, \mu = 0.2564, c = 3.4673$, (a) $n = 1$, (b) $n = 5$, (c) $n = 10$.

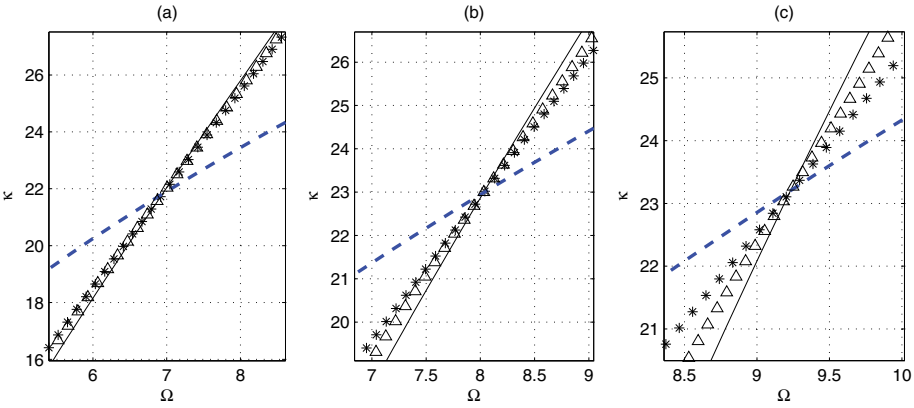

Figure 17: Comparison of asymptotic solution for the coupled PR cut-on wavenumber for all the theories (Section 1 in Fig. (11)) (Eq. (19), Marker '$*$') with the corresponding numerical solution using the Flügge theory (Marker 'Δ') - $h/a = 0.05, \nu = 0.3, \mu = 5.1282, c = 3.4673$, (a) $n = 1$, (b) $n = 5$, (c) $n = 10$. (Also shown are the *in vacuo* flexural wavenumber (Marker '- -') and the uncoupled PR cut-on wavenumber (Marker '—').)

4.2.2 Coupled structural wavenumbers ($\mu \gg 1$)

For the case of $\mu \gg 1$, the coupled longitudinal and coupled torsional wavenumbers are found. The nature of the coupled dispersion relation allows us to find an asymptotic expansion for the coupled wavenumber directly, without having to follow a two-step approach as in the case of $\mu \ll 1$. Thus, we choose a series of the form $\kappa = \kappa_0 + \frac{1}{\mu}a_1 + \nu b_1 + k_\beta c_1$. Substituting this in the coupled dispersion relation and balancing at orders, we obtain the coupled longitudinal wavenumbers.

We present the coupled longitudinal wavenumber for the DM theory followed by the correction terms listed for each of the HOTs.

$$\kappa_{\text{long}} = \sqrt{\Omega^2 - n^2} - \frac{1}{\mu}\frac{n^4 J_n'(\xi_0)\,\xi_0}{2J_n(\xi_0)\,\Omega^4\sqrt{\Omega^2 - n^2}} + k_\beta C, \tag{22}$$

where,

$$C^{\text{LT}} = -\frac{1}{2}\frac{n^2}{\sqrt{\Omega^2 - n^2}},$$
$$C^{\text{GN}} = +\frac{1}{2}\frac{\left(n^2 - 2\Omega^2\right)n^2}{\Omega^2\sqrt{\Omega^2 - n^2}},$$
$$C^{\text{F}} = -\frac{n^2\sqrt{\Omega^2 - n^2}}{\Omega^2},$$
$$C^{\text{K}} = 0.$$

Similarly, the asymptotic expressions for the coupled torsional wavenumbers in the large μ case are as follows,

$$\kappa_{\text{tors}} = \sqrt{2\Omega^2 - n^2} - \frac{1}{\mu}\frac{J_n'(\xi_0)\,\xi_0 n^2\sqrt{2\Omega^2 - n^2}}{2J_n(\xi_0)\,\Omega^4} + \frac{\nu\Omega^2}{\sqrt{2\Omega^2 - n^2}} + k_\beta C, \tag{23}$$

where,

$$C^{\text{LT}} = -\sqrt{2\Omega^2 - n^2},$$
$$C^{\text{GN}} = -\frac{1}{2}\frac{\left(8\Omega^4 - 6\Omega^2 n^2 + n^4\right)}{\Omega^2\sqrt{2\Omega^2 - n^2}},$$
$$C^{\text{F}} = -\frac{\left(3\Omega^4 - 3\Omega^2 n^2 + n^4\right)}{\Omega^2\sqrt{2\Omega^2 - n^2}},$$
$$C^{\text{K}} = 0.$$

The subscripts ‘long’ and ‘tors’ signify the longitudinal and torsional wavenumbers, respectively.

Fig. (18) shows a comparison of the asymptotic expressions for the coupled longitudinal wavenumber with the numerical solution (using the Flügge theory) while Fig. (19) shows a comparison of the asymptotic expressions for the coupled torsional wavenumber with the numerical solution (using the Flügge theory) for each of the four theories for the large μ case. The parameter values chosen are identical to those in Fig. (17).

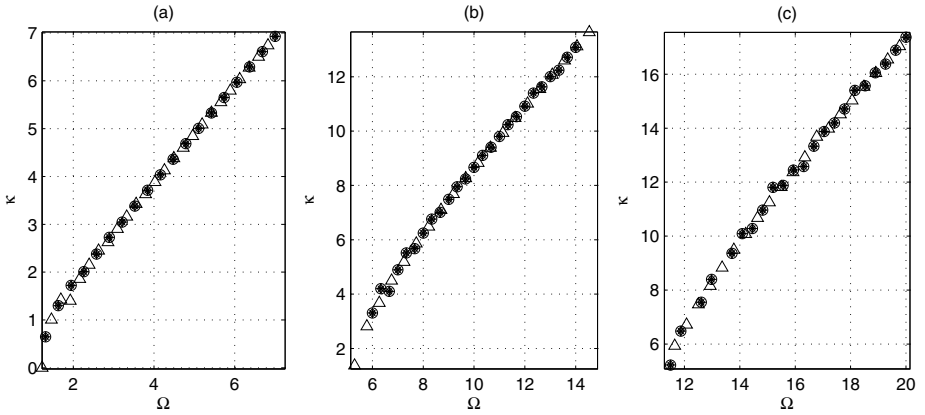

Figure 18: Comparison of asymptotic solution for the coupled longitudinal wavenumber (large μ) for all the theories (Section 2 in Fig. (11)) (Eq. (22)) - Donnell-Mushtari theory (Marker '+'), Love-Timoshenko theory (Marker 'o'), Goldenveizer-Novozhilov theory (Marker '$\times$'), Flügge theory (Marker '$*$') and Kennard simplified theory (Marker '$\diamond$') - with the corresponding numerical solution using the Flügge theory (Marker 'Δ') - $h/a = 0.05, \nu = 0.3, \mu = 5.1282, c = 3.4673$, (a) $n = 1$, (b) $n = 5$, (c) $n = 10$.

Again, similar to the case of light fluid-loading, as seen from the schematic figure for the large μ case (Fig. (11)) and Eqs. (22, 23), the above expansions too break down near the coincidence frequency. However, as seen previously, the expansion is valid upto frequencies very close to the coincidence frequency. Hence, the curves in Fig. (18) appears as a single continuous curve though in reality it too exhibits the 'gap' effect at the coincidence frequency. This 'gap' effect is clearer in the case of the coupled torsional wavenumber for large μ shown in Fig. (19).

The coupled problem is a singular perturbation problem as setting $\mu = \infty$ results in a change in the order of the equation. Thus, it is not possible to find the coupled flexural wavenumbers for $\mu \gg 1$ via a regular perturbation approach.

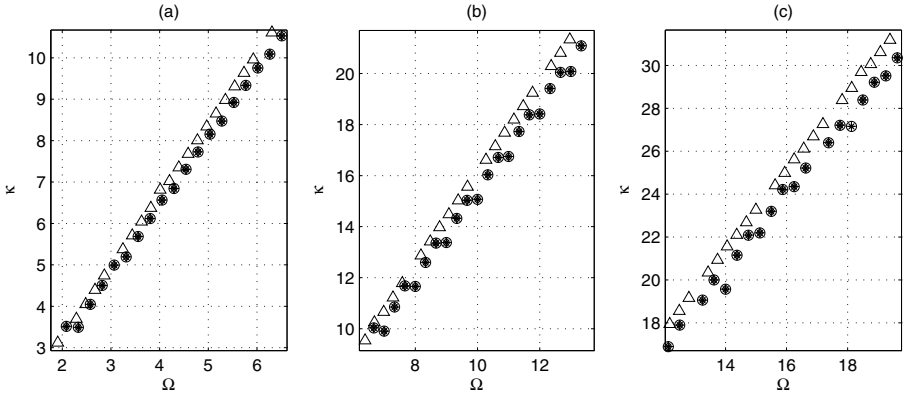

Figure 19: Comparison of asymptotic solution for the coupled torsional wavenumber (large μ) for all the theories (Section 3 in Fig. (11)) (Eq. (23)) - Donnell-Mushtari theory (Marker '+'), Love-Timoshenko theory (Marker 'o'), Goldenveizer-Novozhilov theory (Marker '$\times$'), Flügge theory (Marker '$*$') and Kennard simplified theory (Marker '$\diamond$') - with the corresponding numerical solution using the Flügge theory (Marker 'Δ') - $h/a = 0.05, \nu = 0.3, \mu = 5.1282, c = 3.4673$, (a) $n = 1$, (b) $n = 5$, (c) $n = 10$.

5 Resonance frequencies in finite shells

The approach followed in the previous section is extended to find the resonance frequencies in a circular cylindrical shell of finite length. The case of Shear-diaphragm (SD) - SD boundary conditions at both ends is studied. As noted by Leissa (1973), this is equivalent to attaching two thin flat cover plates at both ends of the shell. As the stiffness of the plates in the in-plane direction is significant, the circumferential (v) and the radial (w) displacement components of the shell at both ends are equal to zero.

The following modeshapes are used

$$u(s,\theta,t) = U\cos(\kappa s)\cos(n\theta)e^{-i\omega t},$$
$$v(s,\theta,t) = V\sin(\kappa s)\sin(n\theta)e^{-i\omega t},$$
$$w(s,\theta,t) = W\sin(\kappa s)\cos(n\theta)e^{-i\omega t},$$

where $s = \frac{x}{a}$ and $\kappa = \frac{m\pi a}{L}$. Substituting these modeshapes in the *pde*s for the shell corresponding to each shell theory, one obtains a sixth order characteristic equation for the non-dimensionalized resonance frequency Ω. This equation for Ω is solved asymptotically using the Poisson's ratio ν and k_β as the asymptotic expansion variables. Thus, a series expansion of the form $\Omega = \Omega_0 + \nu a_1 + \nu^2 b_1 + k_\beta c_1$ is

substituted and the equation is then balanced at each order to yield a final expression for the resonance frequency. Due to the nature of the equation, the form of these expressions is unwieldy for higher circumferential orders ($n \geq 1$) and hence not presented here. The calculations can however be carried out without much trouble using a symbolic math software such as MAPLE. Thus, asymptotic expressions for the resonance frequencies in the axisymmetric mode ($n = 0$) are presented and only the numerical values (obtained after substituting the parameter values in the asymptotic expressions) are presented for higher circumferential orders.

5.1 Axisymmetric mode : $n = 0$

The asymptotic expressions for the resonance frequencies corresponding to the axisymmetric mode are presented below. In the format used until now, resonance frequency expressions corresponding to the Donnell-Mushtari theory are presented first and the corrections to each of the expressions, corresponding to each of the HOTs, are presented subsequently.

$$\begin{aligned}
\text{Axial mode} : \Omega &= \kappa - \nu^2 \frac{1}{2} \frac{\kappa}{[\beta^2\kappa^4 - \kappa^2 + 1]} + k_\beta C_a. \\
\text{Torsional mode} : \Omega &= \frac{1}{2}\sqrt{2}\kappa - \nu\frac{1}{4}\sqrt{2}\kappa - \nu^2\frac{1}{16}\sqrt{2}\kappa + k_\beta C_t. \\
\text{Flexural mode} : \Omega &= \sqrt{\beta^2\kappa^4 + 1} + \nu^2 \frac{1}{2} \frac{\kappa^2}{[\beta^2\kappa^4 - \kappa^2 + 1]\sqrt{\beta^2\kappa^4 + 1}} + k_\beta C_f,
\end{aligned} \tag{24}$$

where $\kappa = \frac{m\pi a}{L}$ and C_a, C_t, C_f are the correction terms corresponding to the axial, torsional and flexural modes, respectively. The forms of the correction terms are listed below in Table 2. for each shell theory.

Correction term	Shell-theory			
	LT	GN	F	K
C_a	0	0	0	0
C_t	$\frac{1}{2}\sqrt{2}\kappa$	$\sqrt{2}\kappa$	$\frac{3}{4}\sqrt{2}\kappa$	0
C_f	0	0	$\frac{1}{2}\frac{1}{\sqrt{\beta^2\kappa^4+1}}$	$\frac{1}{2}\frac{1}{\sqrt{\beta^2\kappa^4+1}}$

Table 2: Correction terms for the resonance frequencies for $n = 0$ (Eq. (24)) for various shell theories.

5.2 Results for higher circumferential orders

Table 3 shows the resonance frequencies for different theories for a thickness ratio of $h/a = 0.05$ for higher circumferential orders. The results for the 3-D elasticity theory were obtained numerically by Leissa (1973) while the results for the other shell theories have been obtained asymptotically. The asymptotic expansions, however, are not presented here as they are cumbersome.

Table 4 shows the percentage error in the resonance frequencies for different theories compared to the result from the 3-D elasticity theory for a thickness ratio of $h/a = 0.05$. The percentage error is calculated as

$$\% \text{ error } = \frac{\text{Shell-theory result (Asymptotic)} - \text{3-D elasticity result (Numerical)}}{\text{3-D elasticity result (Numerical)}} \times 100.$$

6 Conclusions

The question of the relative accuracy of one thin shell theory over another is almost a controversial one and viewpoints on this are widely divergent. Most of the references available in the literature present such a comparison of shell theories for an extreme situation such as buckling of cylindrical shells under axial loads or present resonance frequency calculations for finite shells with certain specified boundary conditions. In this article, we have tried to fill the gap in the available literature by answering this question with regard to wave propagation through infinite *in vacuo* and fluid-filled circular cylindrical shells. In particular we have examined how these five theories compare with each other and how the asymptotic expansions of the wavenumbers also reflect the comparison.

The Donnell-Mushtari (DM) theory is one of the simplest thin shell theories available and hence, in this article, this theory is treated as the base theory and all results are presented as perturbations to the results obtained by using this theory. We start by considering *in vacuo* infinite shells. An appropriate rescaling transformation is applied to the frequency and the wavenumber in order to restrict our attention to specific frequency regions and to specific wavenumber branches, viz., flexural, axial or torsional. This allows us to obtain elegant expansions in each case from which physical insights can be drawn easily. A suitable parameter is also defined such that the governing equations for the higher-order theories can be presented as extensions to the DM theory in terms of this parameter.

Thus, we begin with the *in vacuo* high frequency flexural wavenumber. In this case, the correction at first order arising out of the use of a higher order theory is found to be zero, i.e., the refinement introduced by using a more complex theory over the DM theory is at best a second-order effect. Within the limits of the thin

n	Theory	$l/(ma)$					
		0.1	0.25	1	4	20	100
0	3-D	10.4586	2.2851	0.9580	0.4647	0.0929	0.018586
	D-M	14.2766	2.4702	0.9604	0.4658	0.0932	0.018632
	L-T	14.2766	2.4702	0.9604	0.4659	0.0932	0.018636
	G-N	14.2766	2.4702	0.9604	0.4660	0.0932	0.018640
	Flügge	14.2712	2.4661	0.9598	0.4660	0.0932	0.018638
	K-s	14.2766	2.4702	0.9606	0.4658	0.0932	0.018632
1	3-D	10.4670	2.2938	0.8564	0.2570	0.0161	0.000665
	D-M	14.2909	2.4810	0.8591	0.2573	0.0192	0.0102
	L-T	14.2908	2.4807	0.8584	0.2568	0.0164	0.0051
	G-N	14.2908	2.4806	0.8582	0.2568	0.0164	0.0051
	Flügge	14.2854	2.4767	0.8580	0.2569	0.0165	0.0051
	K-s	14.2909	2.4809	0.8590	0.2571	0.0166	0.0052
2	3-D	10.4914	2.3204	0.6755	0.1213	0.0392	0.0348
	D-M	14.3337	2.5138	0.6801	0.1272	0.0522	0.0516
	L-T	14.3334	2.5128	0.6775	0.1219	0.0409	0.0404
	G-N	14.3333	2.5124	0.6769	0.1216	0.0409	0.0403
	Flügge	14.3281	2.5090	0.6773	0.1218	0.0409	0.0404
	K-s	14.3336	2.5135	0.6791	0.1229	0.0410	0.0404
3	3-D	10.5326	2.3660	0.5393	0.1299	0.1095	0.1092
	D-M	14.4050	2.5700	0.5480	0.1433	0.1236	0.1232
	L-T	14.4044	2.5678	0.5421	0.1312	0.1106	0.1103
	G-N	14.4042	2.5671	0.5410	0.1309	0.1106	0.1103
	Flügge	14.3992	2.5644	0.5419	0.1312	0.1106	0.1103
	K-s	14.4049	2.5692	0.5450	0.1324	0.1107	0.1103
4	3-D	10.5898	2.4323	0.4923	0.2191	0.2090	0.2087
	D-M	14.5050	2.6516	0.5069	0.2348	0.2244	0.2240
	L-T	14.5038	2.6478	0.4970	0.2212	0.2107	0.2104
	G-N	14.5034	2.6467	0.4954	0.2209	0.2107	0.2104
	Flügge	14.4988	2.6448	0.4967	0.2211	0.2108	0.2105
	K-s	14.5047	2.6502	0.5009	0.2219	0.2108	0.2105

Table 3: Resonance frequencies for $h/a = 0.05$ ($a/h = 20$) for various shell theories; '3-D' - 3-D elasticity theory, 'D-M' - Donnell-Mushtari theory, 'L-T' - Love-Timsohenko theory, 'G-N' - Goldenveizer-Novozhilov theory, 'K-s' - Kennard-simplified theory.

n	Theory	$l/(ma)$					
		0.1	0.25	1	4	20	100
0	3-D elasticity	0	0	0	0	0	0
	D-M	36.5061	8.1022	0.2428	0.2498	0.2498	0.2499
	L-T	36.5061	8.1022	0.2428	0.2709	0.2709	0.2710
	G-N	36.5061	8.1022	0.2428	0.2921	0.2921	0.2922
	Flügge	36.4542	7.9233	0.1880	0.2746	0.2815	0.2816
	K-s	36.5062	8.1048	0.2639	0.2428	0.2498	0.2499
1	3-D elasticity	0	0	0	0	0	0
	D-M	36.533	8.1598	0.3124	0.0978	18.947	1438.8
	L-T	36.532	8.1481	0.2346	-0.0631	2.0606	672.74
	G-N	36.532	8.1442	0.2138	-0.0663	2.0605	672.74
	Flügge	36.4805	7.9734	0.1876	-0.0324	2.1372	672.86
	K-s	36.533	8.1580	0.2996	0.0267	2.9097	674.37
2	3-D elasticity	0	0	0	0	0	0
	D-M	36.623	8.3345	0.6847	4.8979	32.967	48.536
	L-T	36.621	8.2895	0.3046	0.5034	4.2406	16.033
	G-N	36.62	8.2749	0.2136	0.2691	4.1654	16.029
	Flügge	36.570	8.1266	0.2714	0.4905	4.2383	16.050
	K-s	36.623	8.3198	0.5324	1.3329	4.5461	16.068
3	3-D elasticity	0	0	0	0	0	0
	D-M	36.766	8.6256	1.6165	10.355	12.866	12.871
	L-T	36.760	8.5307	0.5264	1.0484	1.0248	1.0105
	G-N	36.758	8.5005	0.3121	0.7767	1.0096	1.0099
	Flügge	36.711	8.3856	0.4886	0.9911	1.0386	1.0291
	K-s	36.765	8.5913	1.0524	1.9296	1.0983	1.0356
4	3-D elasticity	0	0	0	0	0	0
	D-M	36.971	9.0147	2.9578	7.1767	7.344	7.3433
	L-T	36.960	8.8607	0.9392	0.9354	0.8310	0.8256
	G-N	36.956	8.8130	0.6263	0.8254	0.8262	0.8254
	Flügge	36.913	8.7368	0.8874	0.9186	0.8490	0.8453
	K-s	36.969	8.9563	1.7306	1.2992	0.8706	0.8504

Table 4: Percentage errors for $h/a = 0.05$ ($a/h = 20$) for various shell theories; '3-D' - 3-D elasticity theory, 'D-M' - Donnell-Mushtari theory, 'L-T' - Love-Timsohenko theory, 'G-N' - Goldenveizer-Novozhilov theory, 'K-s' - Kennard-simplified theory.

shell theory ($h/a = 0.05$), this difference is negligible. In the very high frequency region (for wavelengths of the order of the thickness of the shell), the thin shell approximation breaks down and the error with respect to the 3-D elasticity result is significant. This is also seen in the case of the finite shell for a shell with a very low l/ma ratio. In the low frequency region, the difference between the DM theory and the HOTs is a first order difference. However, on substituting realistic parameter values and plotting the solution, it is seen that the difference in magnitudes is almost negligible. Similarly, in the cases of the high frequency *in vacuo* longitudinal and torsional wavenumbers, whenever there is a non-zero correction term (over the DM theory), its contribution is insignificant for typical parameter values. All the above results have been plotted for an h/a value of 0.05 above which thin shell theory is anyway invalid. For even lower thickness ratios, this difference between the DM theory and the HOTs can be expected to be even smaller.

Next, we consider the wavenumbers in an infinite fluid-filled circular cylindrical shell. The results in this section have been presented in two sections, for small and large values of the fluid-loading parameter, respectively. From the asymptotic expansions, it can be seen that for the coupled acoustic wavenumbers (the coupled RD cut-ons and the coupled PR cut-ons), the difference arising out of the use of a higher order theory to model the structure is a difference of second or higher order. Thus, the use of any thin shell theory is equivalent under such circumstances. For the coupled structural wavenumbers (flexural, longitudinal and torsional), the difference between the theories as seen from the asymptotic expansions is a first order difference. However, within the limits of validity of the thin shell theory this difference is negligible for typical/ realistic parameter values.

From the numerical solutions, it is seen that the difference between the DM theory and the HOTs is indeed significant at very low frequencies (for $n = 1$). However, the asymptotic expansions presented here are rendered invalid in this frequency range and so, no comment can be made. The frequency range over which this significant difference occurs is however small in comparison with the frequency range covered in this paper by the asymptotic expansions. From the perspective of noise generation, this frequency region is mostly not of interest as the sound generated in this region is typically a near-field phenomenon since the wavenumbers are mostly complex.

Finally, a finite shell with Shear Diaphragm - Shear Diaphragm boundary conditions is considered. The approach used so far is extended to finding resonance frequencies. Asymptotic expansions are presented for the resonance frequencies corresponding to the axisymmetric mode. For the higher circumferential orders, the asymptotic expansions are cumbersome and only numerical values for the resonance frequencies (obtained by substituting typical parameter values in the afore-

mentioned asymptotic expansions) and percentage errors (with respect to 3-D elasticity results) are presented.

The novelty of this article lies in presenting all the results as perturbations on the corresponding results for the DM theory, giving one an easy method of quantifying the difference between higher order theories and the DM theory. As mentioned earlier, references in the available literature on the relative accuracies of different thin shell theories under common and non-critical loading conditions are very scarce. This has resulted in the preferential use of more complex theories even when the additional accuracy is insignificant. This also leads to a wastage of computational resources which can be avoided. Secondly, most of the commonly cited references which present a comparison of different thin shell theories via resonance frequency calculations typically present the results for the lowest frequency parameter. Such an approach does not allow the reader to make a prediction regarding the accuracy of higher resonance frequencies. Also, nothing can be said regarding the differing accuracies of the shell theories with respect to a specific type of deformation, viz, flexural, longitudinal or torsional. This information can be especially relevant for particular forcing conditions. Thus, such an approach does not present a complete picture. A study of wavenumbers in an infinite shell employing asymptotic methods to obtain closed form expressions, such as we have carried out, is one way to answer the above criticism convincingly.

References

Donnell, L. H. (1933): Stability of thin-walled tubes under torsion. Technical Report 479, NACA, 1933.

Epstein, P. S. (1942): On the theory of elastic vibrations in plates and shells. *Journal of Mathematical Physics*, vol. 21, pp. 198–209.

Flügge, W. (1962): *Stresses in shells*. Springer Verlag (Berlin).

Fuller, C. R. (1983): The input mobility of an infinite circular cylindrical elastic shell filled with fluid. *Journal of Sound and Vibration*, vol. 87, pp. 409–427.

Fuller, C. R.; Fahy, F. J. (1982): Characteristics of wave propagation and energy distributions in cylindrical elastic shells filled with fluid. *Journal of Sound and Vibration*, vol. 81, pp. 501–518.

Goldenveizer, A. L. (1961): *Theory of thin shells*. Pergamon press (New York).

Kennard, E. H. (1953): The new approach to shell theory : Circular cylinders. *Journal of Applied Mechanics*, vol. 20, pp. 33–40.

Kennard, E. H. (1955): Cylindrical shells : Energy, equilibrium addenda and erratum. *Journal of Applied Mechanics*, vol. 22, pp. 111–116.

Kennard, E. H. (1956): Approximate energy and equilibrium equations for cylindrical shells. *Journal of Applied Mechanics*, vol. 23, pp. 645–646.

Kennard, E. H. (1958): A fresh test of the epstein equations for cylinders. *Journal of Applied Mechanics*, vol. 25, pp. 553–555.

Kunte, M. V.; Sarkar, A.; Sonti, V. R. (2010): Generalized asymptotic expansions for coupled wavenumbers in fluid-filled cylindrical shells. *Journal of Sound and Vibration*, vol. 329, pp. 5356–5374.

Kunte, M. V.; Sarkar, A.; Sonti, V. R. (2011): Generalized asymptotic expansions for the wavenumbers in infinite flexible in vacuo orthotropic cylindrical shells. *Journal of Sound and Vibration*.

Leissa, A. (1973): Vibration of shells. Technical Report NASA SP-288, 1973.

Love, A. E. H. (1944): *A treatise on the mathematical theory of elasticity*. Dover Publications, Inc.

Mushtari, K. M. (1938): On the stability of cylindrical shells subjected to torsion. *Trudy kaz. avais*, vol. 2.

Novozhilov, V. V. (1964): *The theory of thin elastic shells*. P. Noordhoff Lts (Groningen, The Netherlands).

Sarkar, A.; Sonti, V. R. (2007): An asymptotic analysis for the coupled dispersion characteristics of a structural acoustic waveguide. *Journal of Sound and Vibration*, vol. 306, pp. 657–674.

Sarkar, A.; Sonti, V. R. (2007): Asymptotic analysis for the coupled wavenumbers in an infinite fluid-filled flexible cylindrical shell : The axisymmetric mode. *Computer modeling in Engineering and Sciences*, vol. 21, no. 3, pp. 193–207.

Sarkar, A.; Sonti, V. R. (2009): Asymptotic analysis for the coupled wavenumbers in an infinite fluid-filled flexible cylindrical shell : The beam mode. *Journal of Sound and Vibration*, vol. 319, pp. 646–667.

Timoshenko, S. P. (1959): *Theory of plates and shells*. McGraw-Hill (New York).

Venkatesham, B.; Pathak, A.; Munjal, M. L. (2007): A one-dimensional model for prediction of a finite rectangular duct with different acoustic boundary conditions. *International Journal of Acoustics and Vibration*, vol. 12, pp. 91–98.